# Study of Mode Transition in Three-dimensional Laser Beam Oscillating Welding of Aluminum Alloy

Zhenyu Liu[a,b], Peilei Zhang[a,b,c*], Mingliang Yan[a,b], Zhishui Yu[a,b*], Yingtao Tian[d] , Di Wu[a,b]

[a]School of Materials Engineering, Shanghai University of Engineering Science, Shanghai 201620, China

[b]Shanghai Collaborative Innovation Center of Laser of Manufacturing Technology, Shanghai 201620, China

[c]Fraunhofer Institute for Laser Technology ILT, Aachen 52074, Germany

[d]Department of Engineering, Lancaster University, Lancaster LA1 4YW, United Kingdom

Keyword: oscillation laser welding, transition of heat-conduction mode and keyhole mode, calculation of threshold temperature of keyhole mode, aluminum alloy

**Abstract**

Although 2-d (two-dimensional) beam oscillation can reduce the porosity defects during laser welding of aluminum alloys, it distributes the heat input, resulting in a higher power required to form a capillary. Therefore, this research draws attention to an alternative approach, which is considered to be beneficial to laser absorption in oscillation laser beam welding, 3-d (three-dimensional) oscillation of the laser beam. (3-d oscillation means that the laser spot moves on the two-dimensional plane and the defocus change simultaneously, causing the heat input to change) An experiment was designed where the variation of oscillation frequency leads to significant changes in capillary behavior. The result shows that the increase of vertical oscillation can promote the formation of a capillary. When the oscillation frequency reaches some special values, the capillary appears and disappears periodically, such as the vertical oscillating frequency is 5Hz, rotation oscillating frequency is 200Hz. Meanwhile, welding pores are generally distributed at the position where the capillary begins to disappear. The reason for promoting capillary formation during 3-d laser beam oscillation, and the change of normalized temperature, which is meaningful for understanding the welding mode transition, is illustrated by a simplified model. Compared with traditional linear welding, the experimental results show that it is possible to obtain lower porosity seam during 3-d laser beam oscillation welding in low feed rate, and the mechanism of stabilizing the molten pool is discussed qualitatively

* Corresponding authors: Peilei Zhang (peilei@sues.edu.cn) and Zhishui Yu (yu_zhishui@163.com)

## 1. Introduction

It is still a challenge that deep penetration laser beam welding of common aluminum alloys due to the formation of process pores. Tsay et al. (2006) proposed that large porosity strongly affects the strength and fatigue property of weld joints. Meanwhile, the keyhole behavior is related to the formation of welding pores. Berger et al. (2011) found that porosity is mostly caused by an unstable vapor capillary. Fetzer et al. (2018) showed series of images by online X-ray, suggested that the repeating cycle of bulging of the capillary and transition of that bulge as a bubble into the melt pool are the causes of aluminum alloy welding porosity.

Among various solutions to reduce welding defects, oscillating laser welding is suitable for modern production. Compared with the laser-arc hybrid welding, due-beam welding, wire filling welding, mechanical oscillation welding, in oscillation laser welding, the laser spot could be oscillated periodically through scanning mirrors, without introducing a third field. Rodrigues et al. (2018) improved the On-The-Fly technology, a handling system with coupled axes consisting of a conventional industrial robot and a high-power beam deflection optics for oscillation laser beam welding, from the view of electrical engineering. Kumar et al. (2021) applied oscillation laser welding technology in the battery field. These researches indicated that oscillation laser welding was easy to automate.

Some researchers point out that in oscillating welding, the laser energy distribution could be predetermined by the oscillating trajectory, and the energy distribution significantly affects the weld formation, grain refinement, molten pool behavior and pores suppression. Hao et al. (2015) found that with the increasing of laser oscillating amplitude and frequency, the penetration depth and melting width at the bottom changed because the transition of welding mode changed. Wang et al. (2019) found that there are significant weld formation differences between welds produced by different oscillation trajectories. Jiang et al. (2020) proposed that the accumulation of laser energy near the weld center was more beneficial to the growth of equiaxed grains. Zhang et al. (2020a) established a finite element model to study rotation oscillating welding and pointed out that the temperature gradient of the melt pool is reduced when the oscillation frequency and amplitude increase. In their next work, Zhang et al. (2020b) proposed that a stable eddy caused by laser-induced keyhole velocity plays an essential role in welding pores suppression.

3-d (three-dimensional) laser beam oscillation welding is a new kind of oscillation welding, which provides a new idea for changing energy distribution. 3-d oscillation means that the laser spot moves on the two-dimensional

plane and the defocus changes simultaneously, causing the heat input to change. In a few research on 3-d oscillating welding, Wu et al. (2018) proposed that vertical oscillation amplitude increase the penetration depth but the coupling between vertical oscillation and rotation oscillation is no systematic study, and the disparity between 2-d oscillation and 3-d oscillation in this study is small because the oscillation frequency is not getting enough attention. So it is meaningful to study the 3-d oscillating welding more deeply, especially the role of oscillation frequency in 3-d oscillating welding.

Meanwhile, the energy input in 3-d oscillating welding changes simultaneously, which is similar to laser power modulation welding and 3D printing. Martin et al. (2019) pointed out that when the laser spot turns around in the corner the capillary becomes unstable and the pores are formed. This indicated that the calculation of the keyhole mode threshold is necessary to obtain a stable welding process. Ning et al. (2019) showed that the optimized modulated-power laser welding could change the energy distribution and obtain a deep keyhole with long life. Fetzer et al. (2021) announced that a stable wedge-like geometry was found at high feed rates, and the laser radiation is absorbed mostly at the front wall of the capillary. These researches provide us an idea to obtain a stable keyhole by controlling the laser energy distribution in keyhole.

In the current laser welding technology of aluminum alloy, laser welding with a high scanning speed and a high feed rate can effectively suppress porosity and obtain large weld depth, but it needs high power laser. 2-d oscillation laser welding technology can reduce porosity at low feed rates, but the penetration depth in 2-d oscillation laser welding is smaller. This research draws attention to an alternative approach, 3-d (three-dimensional) oscillation of the laser beam. In this paper, a transition of welding mode caused by ascending vertical oscillation frequencies is found. Combining the high-speed imaging method and the simulation results of temperature field, the reason for the mode transition caused by the laser 3-d oscillation was analyzed. According the observation of keyhole based on a "half sandwich" model, the pore distribution and laser energy distribution in keyhole were studied. This work can promote the development of 3-d laser beam oscillation welding.

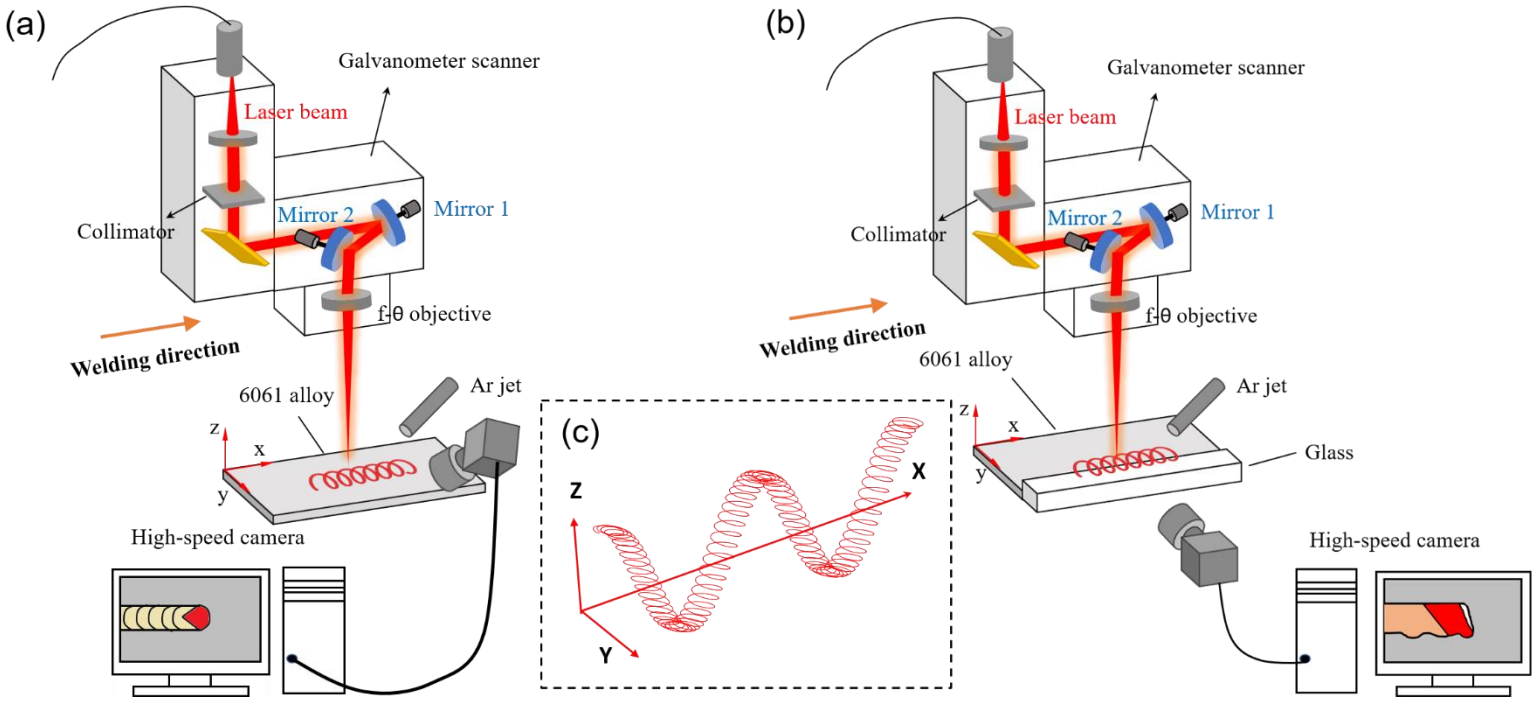


Fig 1. Schematic of the experimental setup and 3-d laser beam oscillating trajectory. (a) weld pool observation; (b) keyhole observation based on the " half sandwich" model; (c) 3-d laser oscillating trajectory.

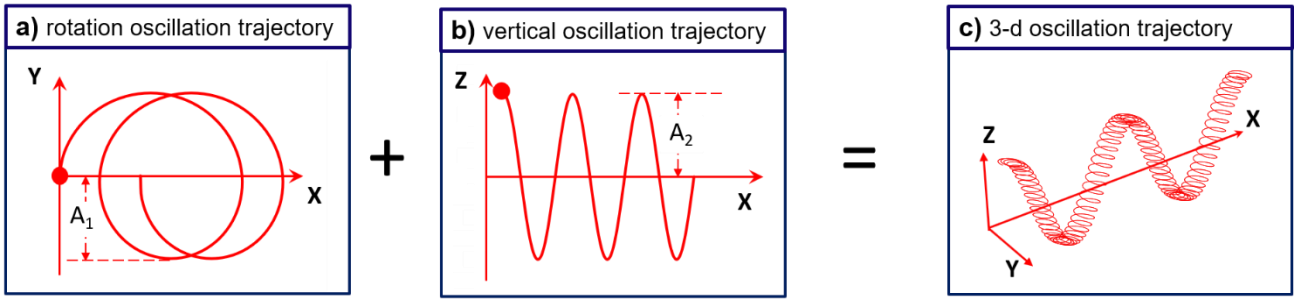


Fig 2. Process of inferring the 3-d oscillation trajectory.

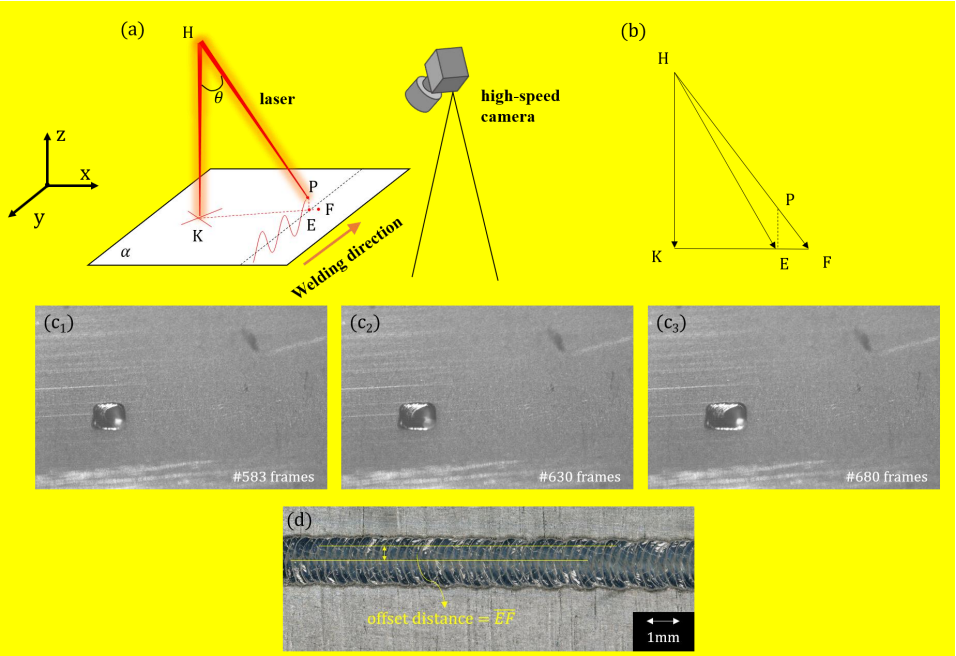


Fig 3. Schematic diagram and result of a confirmatory experiment about amplitude and frequency in vertical oscillation. (a) Schematic diagram; (b) geometric relationship between offset distance and oscillation amplitude; ($c_1$-$c_3$) Snapshot of high-speed video during two oscillation cycles; (d) weld surface morphology used to calculated the actual amplitude.

## 2. Experimental procedures

The welding system used for 3-d oscillation welding was equipped with a Blackbird intelliWELD II FT galvanometer scanner, an IPG YLS-5000 fiber laser, and an ABB IRB 4600 robot in ambient air at room temperature. **Fig. 1c** is a schematic diagram of the 3-d oscillating trajectory. As is shown in Fig. 2, The three-dimensional oscillation welding is the vector sum of rotation oscillating on work plane and vertical harmonic oscillating. As the focus moves on the rotation oscillating path, the defocus changes as a cosine function. The 3-d oscillating trajectory can be described by equations (1-3).

$$x = v_0 t + A_1\left(1 - cos2\pi f_{xy} t\right) \quad (1)$$

$$y = A_1 \sin(2\pi f_{xy} t) \quad (2)$$

$$z = A_2 \cos(2\pi f_z t) \quad (3)$$

Where $f_z$ , $f_{xy}$ represents the vertical harmonic oscillation frequency and rotation oscillation frequency respectively, and the feeding speed is $v_0$. As is shown in Table 1, if there is no additional explanation, in this paper, the amplitude $A_1$ = 0.5mm, $A_2$ = 2mm, with laser power of 3.68kW and welding speed of 3m / min.

As shown in Fig. 1(a) and Fig. 1(b), the laser beam wavelength is 1060nm and the fiber diameter is 200μm. The scanner includes a collimating lens with a focal length of 450mm and an f-θ focusing objective with a focal length of 150mm. The focal diameter $R$ of the laser beam is 0.6mm. Refer to the “sandwich” experiment model of

Huang et al. (2018), The base material 6061 Aluminum alloy used in this study in the dimension of 50mm (length) × 30mm (width) × 5mm (thickness) and the heat resistant quartz glass in the dimension of 50mm (length) × 30mm (width) × 6mm (thickness). The 0 defocus plane of the laser beam was set on the upper surface of the Aluminum plate, and in the "half sandwich method", the weld is located at the butt joint between the base plate and heat resistant glass.

Table 1 Welding parameters

| Parameters | Unit | Values |
|---|---|---|
| Laser power | W | 3680 |
| Feeding speed | mm $s^{-1}$ | 50 |
| Ar flow rate | L $min^{-1}$ | 10 |
| Vertical oscillating amplitude | mm | 2 |
| rotation oscillating amplitude | mm | 0.5 |

The high-speed charge-coupled device (CCD) camera used was a Phantom VEO 640 with a resolution of 832 × 600 is placed at different positions to detect the keyhole and weld pool behaviors. This process is carried out with a diode laser (Cavilux Smart) to illuminate the weld to obtain clear images. The sample rate is 10000 frames/s.

Additionally, a confirmatory experiment is used to confirm the amplitude and frequency that optics can achieve in vertical oscillation. As is shown in Fig. 3(a), a laser incident angle $\theta$ is intentionally designed, and the welding trajectory is shown by the red solid line in Fig. 3(a), which is a cosine curve with 0 z-coordinate value at the center. In the confirmatory experiment, the laser is focused on point P but point F is where to be welded actually. In a word, the laser incident angle in vertical oscillation laser beam welding causes the offset of actual welding position. A geometric relationship proposed in Fig. 3(b) showed that the actual amplitude can be calculated by measuring the distance of segment EF. As is shown in Fig. 3(d), the offset distance is measured and the actual amplitude in 200 Hz is calculated as 1.93 mm, which is close to 2mm and tolerable if the measurement error is considered. Meanwhile, the snapshot showed that the number of frames between two adjacent oscillation cycles is about 50, so the cycle time of oscillation is obtained by dividing the number of frames by the sample rate, and the 200 Hz frequency is confirmed.

Before welding, the surface of the aluminum alloy was ultrasonically cleaned in acetone for 15 minutes to

remove the contaminants adhering to the surface and then dried in a drying oven at 150°C for 2 hours. Each metallographic specimen was ground, polished, and etched with 4 ml of $HNO_3$ and 96 ml of $CH_3CH_2OH$ solution. The microstructure and fracture morphology of the joints were analyzed by optical microscopy.

## 3. Experiment result and discussion

This paper mainly studies the transition of welding mode in 3-d oscillation welding. In 3.1, the disadvantage of 2-d oscillation welding has been shown, and the change in oscillation frequency even causes the transition of welding mode. In 3.2, a model described the above welding mode transformation is established. In 3.3, the relationship between oscillation frequency and welding porosity is qualitatively discussed.

### 3.1. Benefits in increasing penetration and transition of welding mode during 3-d oscillation welding.

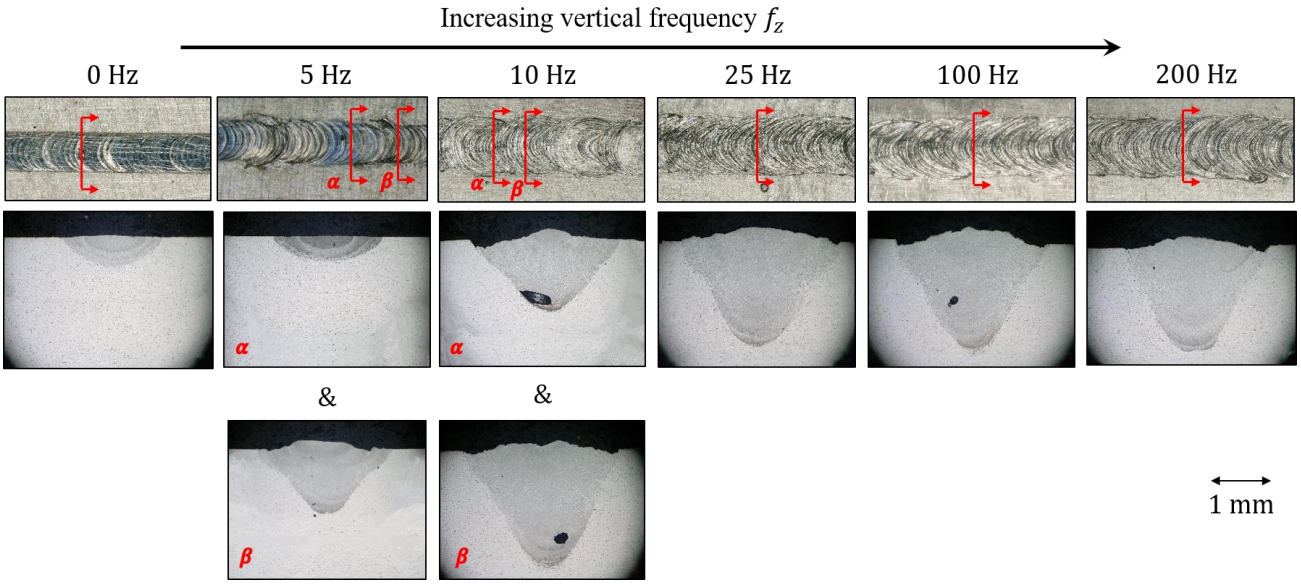


Fig. 4. Morphologies of top surface and cross-section at the different vertical oscillating frequencies

Fig .4 shows the top surface morphology and cross-section at different oscillating frequencies. With the increase of vertical oscillation frequency, the fish scale-shaped ripples change from bright silver fish scale-shaped ripples to gray-white fish scale-shaped ripples. Meanwhile, the melt width and melt depth increase gradually, and keep stable after the vertical frequency reached 25Hz. Specially, when $f_z = 5\text{Hz}$, $f_{xy} = 200\text{Hz}$ and $f_z = 10\text{Hz}$, $f_{xy} = 200\text{Hz}$, the top surface morphology at different positions are different in the seam, So as the cross-section. While vertical frequency $f_z = 5\text{Hz}$ and rotation frequency $f_{xy} = 200\text{Hz}$, the color of fish scale-shaped ripples switched between bright silver and gray-white, and the weld cross-section under the bright silver ripples shows an almost heat-conduction weld shape whereas the weld cross-section under gray white ripples has a typical

keyhole mode shape as shown in Fig. 5(c). For convenience, the welding mode on which weld switching between keyhole mode and heat-conduction mode is referred to as SBHK mode (switching between heat-conduction mode and keyhole mode) in this paper.

While vertical frequency $f_z = 10\text{Hz}$ and rotation frequency $f_{xy} = 200\text{Hz}$, the weld fusion lines are wavily, and the penetration depth on the peak is significantly higher than that at the valley. In previous research, Jia et al. (2021) welded the 6061 aluminum alloy by a pulse laser, in which the weld fusion lines is similar to this paper, indicating that the energy input is quite different at those points, and the reason caused energy input change may be the transition of welding mode.

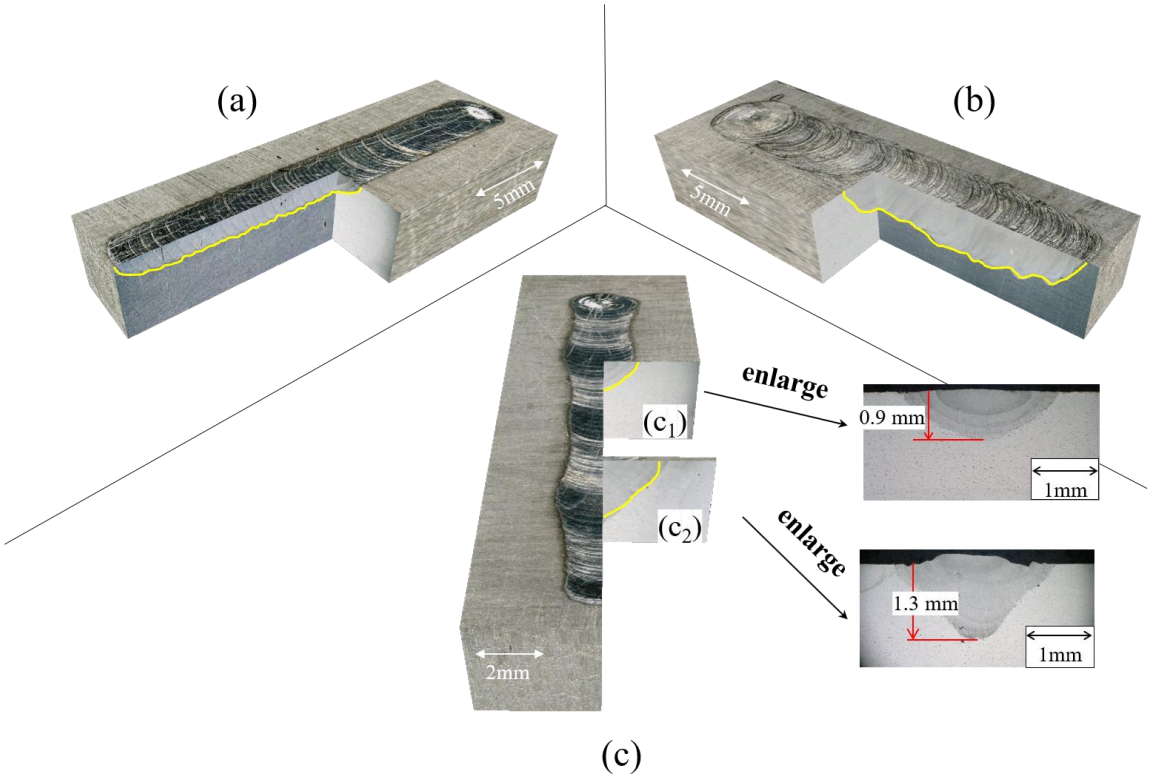


Fig 5. Three mode in the weld of laser beam 3-d oscillating, and metallographic section; (a) heat-conduction mode ($f_z = 0Hz$, $f_{xy} = 200\text{Hz}$); (b) keyhole mode ($f_z = 200\text{Hz}$, $f_{xy} = 200\text{Hz}$); (c) switching between heat-conduction mode and keyhole mode (SBHK mode) ($f_z = 5\text{Hz}$, $f_{xy} = 200\text{Hz}$)

A series of high-speed photographs in Fig. 6 shows the relationship between the transformation of welding mode and weld pool behavior. In Fig. 6(a-c), if there is a keyhole in the molten pool, the molten metal near this position will form gray-white fish scale-shaped ripples after solidification, on the contrary, bright white fish scale-shaped ripples will be formed, which means that the difference of laser energy input is due to the change of welding mode—in keyhole mode, the energy absorbability is high. The temperature behind the molten pool is

higher than that during heat-conduction welding, so the fluctuation of molten pool is more serious than which one in heat-conduction mode because of the Marangoni effect. These lead to the fluctuation at the solidification front of the weld. Due to the relationship between reflection and surface morphology, the color of the fish scale is different. Similarly, the change of weld fusion width is also related to welding mode. Cheng et al. (2021) found the increase of melt width when the welding mode changed. Furthermore, as shown in Fig. 6(d-e), while the vertical oscillating frequency increase to 25Hz, the heat-conduction welding mode disappears. The keyhole appeared at the beginning and disappeared only after the laser came out.

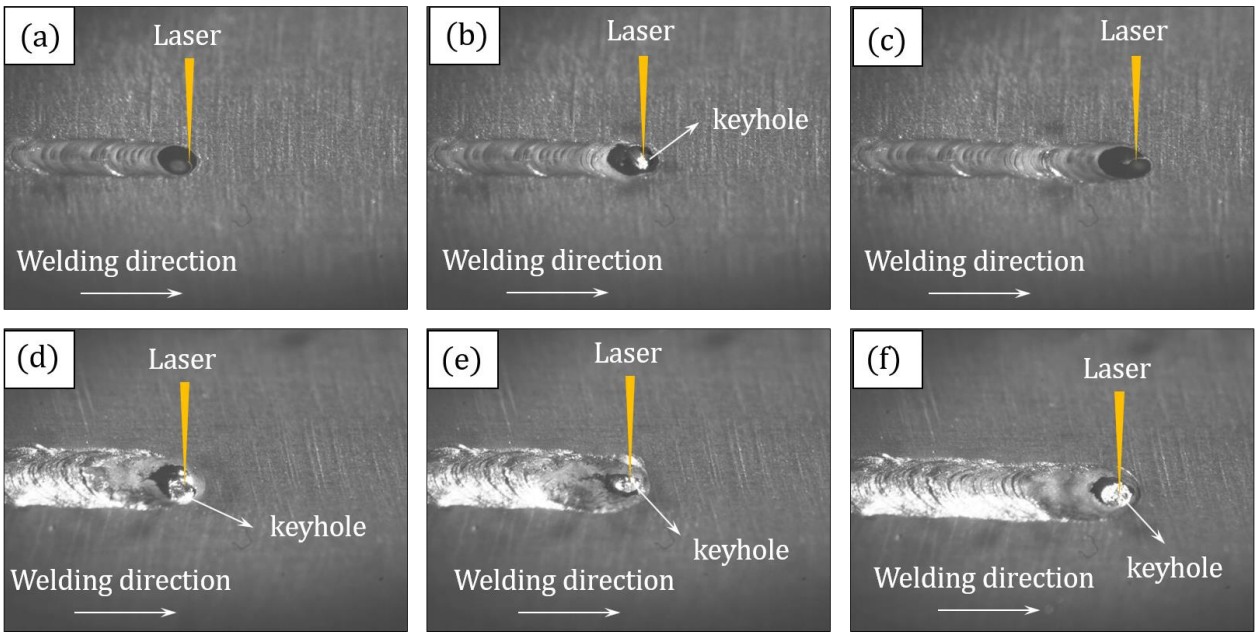


Fig 6. High speed photographs of the weld pool. vertical oscillating frequency $f_z = 5$Hz, rotation oscillating frequency $f_{xy} = 200$Hz in (a)-(c). vertical oscillating frequency $f_z = 25$Hz, rotation oscillating frequency $f_{xy} = 200$Hz in (d)-(f). (a) $t = 0.1875$ s; (b) $t = 0.2125$ s; (c) $t = 0.245$ s; (d) $t = 0.1875$ s; (e) $t = 0.2125$ s; (f) $t = 0.245$ s.

More data of welding mode in 3-d oscillating welding was collected in Fig. 7. It is clear from Fig. 7 that when the vertical oscillation frequency is low, and the rotation oscillation frequency is high, the weld is on heat-conduction mode; when the vertical oscillation frequency is high, and the rotation oscillation frequency is low, the weld is on keyhole mode; the weld is on SBHK mode when the oscillation frequency is in the middle. Which is surprising is that when the vertical oscillation increase, the mode change from heat-conduction mode to keyhole mode. It seems like the vertical oscillation seems to increase the laser absorptivity. Stritt et al. (2011) utilized laser power modulation to investigate the transition from heat-conduction to deep-penetration welding, it is found that the spot size was inversely proportional to the threshold of keyhole formation. Based on the research of Stritt et al. (2011), we can make the following hypothesis, which is well consistent with the phenomena in the experiment:

The vertical oscillation of the laser beam has a similar effect to the laser spot modulation. While the laser spot is large, the dispersed energy is not enough to form a keyhole; while the laser spot is small, the concentrated energy makes the center of the molten pool begin to gasify and form a depression. In section 3.2 of this paper, the discussion is analyzed and graphical by calculating the temperature field in a finite region.

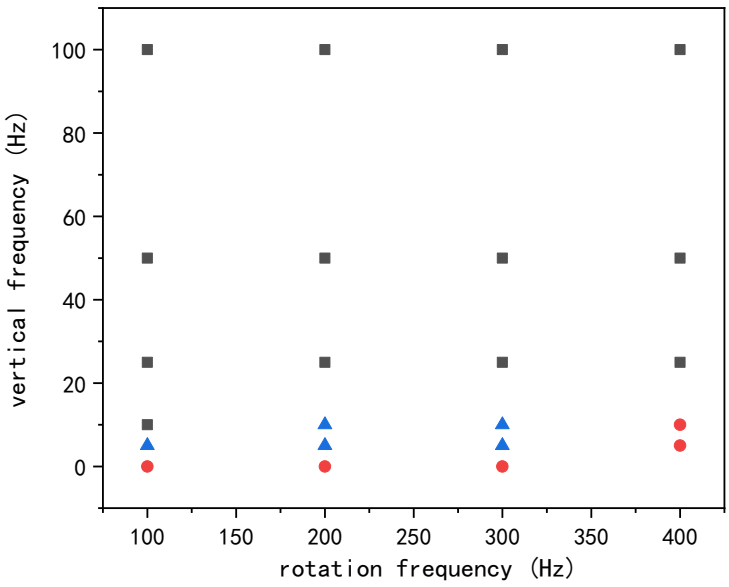


Fig 7. Relationship between the oscillating frequency and welding mode. The square points represent the welding is on keyhole mode; The circular points represent the welding is on heat-conduction mode; The triangle points represent the welding is switching between heat-conduction mode and keyhole mode.

In addition, when the welding mode is switching between heat-conduction mode and keyhole mode, the capillary appears and disappears periodically. As is shown in Fig. 8, the keyhole existed in the molten pool when bonding time is 0.1814s, after about 3 milliseconds, the keyhole disappeared and porosity was found at the same position. Lin et al. (2017) considered that the unstable keyhole is an important cause of porosity in aluminum alloy laser welding. Zhao and DebRoy (2003) showed that there are large pores in the seam when the welding mode changes from heat-conduction mode to keyhole mode. Therefore, in order to produce welds with low porosity, the SBHK mode should be avoided.

In general, it can be qualitatively understood from the above discussion: first, rotation oscillation has the disadvantage of dispersing heat input, which makes the welding can only be carried out in heat-conduction mode when the laser power is about 3.68kW; Second, as if vertical oscillation frequency increases and the frequency of rotation oscillation keep a constant value, the welding mode transfers from heat-conduction mode to keyhole

mode. Which conflict with the traditional theory such as surface energy density $P/V_s r_0$, and volumetric energy density $P/V_s {r_0}^2$ , is that the addition of vertical oscillation makes $r_0$ larger in the above formula, but seems to have the ability to promote the formation of a keyhole.

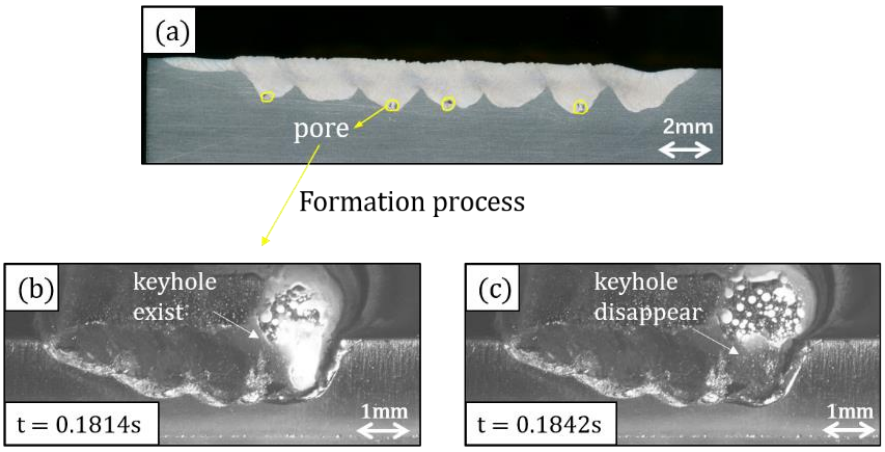


Fig 8. Formation process of porosity when the welding is on SBHK mode (switching between heat-conduction mode and keyhole mode), the vertical oscillation frequency $f_z$ is 10Hz, the rotation oscillation frequency $f_{xy}$ is 200Hz

3.2. Model and theoretical calculation

Next, this paper will analyze the following two issues in 3.2: first, in the welding process with 3.68kW power, 50mm/s scanning speed, 200Hz rotation frequency and 0.5mm rotation radius, the welding mode is always in the thermal conductivity welding mode. After adding 5Hz cosine vertical oscillation, the welding mode switch on heat conduction mode. This is against the previous theory because vertical oscillation will make laser beam defocus, which is not conducive to the generation of a keyhole in the previous theory. Second, when the cosine vertical oscillation frequency is increased, the heat conduction welding mode disappears in the welding process, and none of the current deep penetration welding criteria adapt to 3-d laser oscillation welding.

The model is based on the following preconditions:

(i) We begin with a heat conduction problem in a finite region without considering the Marangoni flow, Melting enthalpy, evaporation and spattering. Graf et al. (2015) showed that energy loss because of evaporation and spattering can be ignored in heat-conduction mode. Gan et al. (2021) showed that energy loss due to melting enthalpy can be ignored as comparison with heat conduction.

(ii) Temperature-independent thermophysical properties at the melting point are assumed to be in the derivation. Ke et al. (2021) claimed that the inclusion of the temperature-dependent thermophysical properties does not change the temperature field qualitatively in aluminum alloy welding.

(iii) If there is no keyhole in the molten pool, the effect of defocusing on welding is equivalent to the spot size

modulation, which means that the attenuation of laser energy propagating in the air is ignored.

We consider a laser beam scanning a substrate with the scan speed $v_0$ along direction $x$. Direction $y$ is the transverse coordinate, and $z$ is the normal into the substrate surface. The temperature field is governed by

$$\rho C_p \frac{\partial T}{\partial t} = \nabla(k_0 \nabla T) + Q \tag{4}$$

where $\rho$ is the density of the solid, $C_p$ is the heat capacity, $k_0$ is the Boltzmann constant. $T$ is the temperature.

The boundary condition considering a Gaussian heat source can be expressed as:

$$\lambda \frac{\partial T}{\partial z} = \frac{2\eta P}{\pi r_0^2} \exp\left[\frac{-2((x-x_0)^2 + (y-y_0)^2)}{r_0^2}\right], z = 0 \tag{5}$$

$$r_0 = r_s \times \sqrt{1 + (\frac{z_0^2}{1.6^2})} \tag{6}$$

$$T = T_0, d \to \infty \tag{7}$$

Where $\eta$ is the effective laser absorptivity, $P$ is the laser power, $\lambda$ is the thermal conductivity, $T_0$ is the preheat temperature, and $d$ is defined as $d = \sqrt{x^2 + y^2}$, $r_0$ is the laser spot radius, equation 6 is used to describe the relationship between the Z coordinate value of the focus and the spot size in 3-d oscillation, and equation 6 is obtained by measuring and fitting the spot defocus from -5mm to 5mm. $x_0, y_0, z_0$ are the 3-d coordinate values of the laser focus, which are given by the trajectory equation (1-3). In heat transfer, thermal diffusivity $\alpha$ is used frequently, which is equal to $\lambda/\rho C_p$. The thermo-physical material properties were shown in Table 2.

For some certain points near point A and point B, their temperature change curve can be obtained through making the space term $\nabla(k_0 \nabla T) = 0$ in the control equation 4, and obtained:

$$T(x,y,0,t) = \frac{\eta P}{\pi\lambda}\sqrt{\frac{\alpha}{\pi}} \int_0^t \frac{dt}{\sqrt{t}(4\alpha t + ({}^{r_0^2}/_2))} \times \exp\left[-\frac{z^2}{4\alpha t} - \frac{(x-x_0)^2 + (y-y_0)^2}{4\alpha t + \left({}^{r_0^2}/_2\right)}\right] \tag{8}$$

Table 2. Thermo-physical material properties used in this paper

| Parameters | Unit | Values |
|---|---|---|
| Density | Kg $m^{-3}$ | 2660 |
| Heat capacity | J $kg^{-1}$ $K^{-1}$ | 1050 |
| Thermal conductivity | W $m^{-1}$ $k^{-1}$ | 90 |

| | | |
|---|---|---|
| Surface tension | $N\ m^{-1}$ | 0.3 |
| Effective laser absorptivity | | 0.12 |

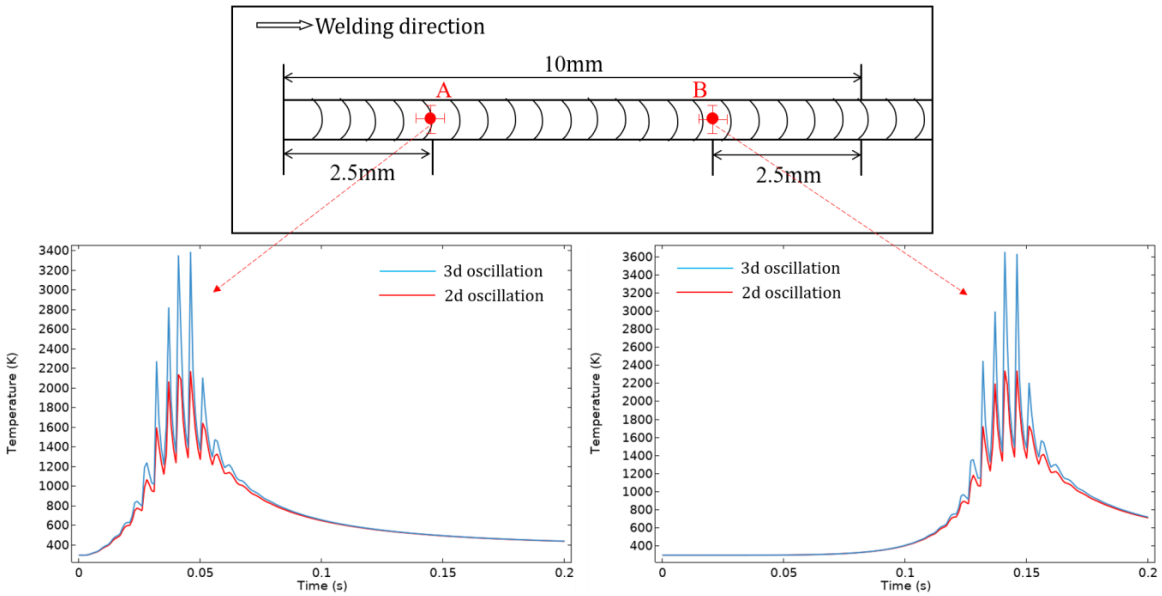


Fig 9. Temperature curve of point A and point B with different kind of laser oscillation.

Fig. 9 shows the average temperature curves of four points around point A and point B. These four points are 0.2mm near point A and point B. As shown in Fig. 9, the maximum temperature near point A and point B in 3-d oscillation welding is higher than that of point A and point B in 2-d oscillation welding. To understand, the temperature curve is explained in the energy distribution diagram shown in Fig. 10, and the color represents the laser energy density. Compared with the change of spot size in Fig. 10(a) and Fig. 10(b), when the spot is large, the heat flow is dispersed, and the welding is in the heat conduction welding mode. When the spot becomes smaller and the heat flow is concentrated, the welding mode changes from heat conduction mode to keyhole mode. At the same time, compared with the 2-d oscillation welding, the large laser spot in the 3-d oscillation is conducive to the conduction of heat flow to the distance, so some points at specific positions in the weld receive more heat flow than in the 2-d oscillation, resulting in the transformation of welding mode. In order to understand the differences of energy distribution between 3-d oscillation laser beam welding and 2-d oscillation laser beam welding, an energy distribution diagram is given, and the area of high energy density has been extracted. As is shown in Fig. 9(c) and Fig. 9(f), the area in which energy density higher than 700 $J/mm^2$ in 3-d oscillation laser beam welding is concentrated near the center of the weld. At the same time, the area in which energy density higher than 700 in 2-d

oscillation laser beam welding is close to the edge of fusion line. It means that the fusion metal near the center of the weld pool get more energy input than the one close to the fusion line. Meanwhile, the video of keyhole generation is given in Fig. 11. As is shown in Fig. 11, the keyhole always forms around the center of molten pool. It means that compare to the edge of molten pool, heating the center of molten pool is easily to produce a keyhole, because the edge of molten pool is more likely to lose heat due to its proximity to the base metal when heat conduction plays a major role.

It is worth mentioning that, the temperature curve in Fig. 8 should be higher than the actual temperature, because the melting phase transformation is ignored in the above analysis. However, we observed that when the welding is in SBHK mode, the amount of molten metal is similar to that of heat-conduction mode due to the short duration of keyhole. Therefore, it is tolerable to ignore the melting phase transition in comparing the maximum temperature in 3-d and 2-d oscillating welding.

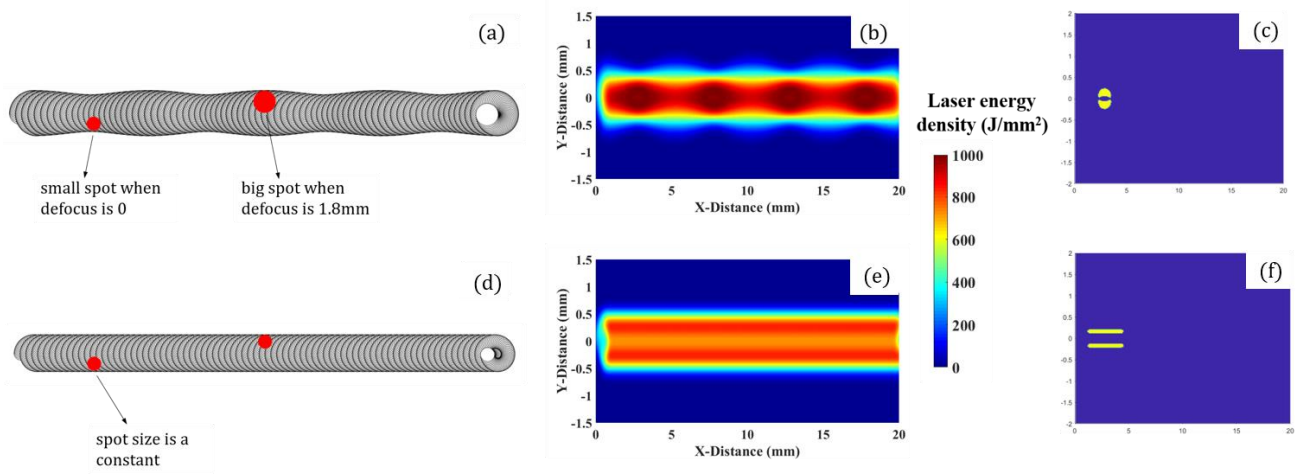


Fig 10. (a) Schematic diagram of the change of spot size in 3-d oscillation welding ($f_{xy}$= 200 Hz, $f_z$= 5 Hz); (b) Energy distribution in the weld of 3-d oscillation ($f_{xy}$= 200 Hz, $f_z$ = 5 Hz); (c) The area in 3-d oscillation laser beam welding, in which the energy density is larger than 700 J/mm2 (d) Schematic diagram of the change of spot size in 2-d oscillation welding ($f_{xy}$ = 200 Hz, $f_z$ = 0 Hz); (e) Energy distribution in the weld of 2-d oscillation ($f_{xy}$ = 200 Hz, $f_z$ = 0 Hz); (f) The area in 2-d oscillation laser beam welding, in which the accumulated energy is larger than 700 J/mm$^2$

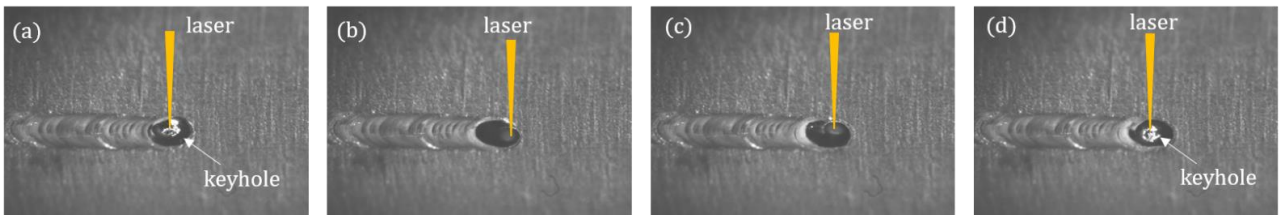


Fig 11. High-speed photography of molten pool during keyhole formation (a) 0.22 s; (b) 0.225 s; (c) 0.23s; (d) 0.235s.

Another issue is when vertical oscillation increase, the welding mode changed from SBHK mode to keyhole mode. And how to describe the threshold of keyhole mode in 3-d oscillation welding.

Stritt et al. (2011) found that the keyhole formation threshold is higher than keyhole disappearance threshold. It means that when the energy input in the keyhole reaches the threshold, the keyhole will not disappear immediately, which is seems like the keyhole has a "delay". Ning et al. (2019) proposed that the reason for the "delay" is that there was still enough recoil pressure at the bottom of keyhole to counteract surface tension. Therefore, this paper attempts to describe the threshold of keyhole mode by a force balance model based on self-focus effect.

In addition to the above assumptions i ,ii and iii, the following assumptions are added:

(iv) In this paper, the condition for forming a keyhole is that the micro depression on the surface of the molten pool reaches a certain depth, at which the incident laser just self focuses. When the depression exceeds this depth, the self-focusing laser will lead to a sharp increase in the laser absorption rate of the molten pool and enter the deep penetration welding mode. Zou et al. (2015) successfully predicted the keyhole welding transformation of A3 steel using this model. For 6061 aluminum alloy with higher reflectivity, this model is accurate within the error tolerance.

(v) Ignoring the interaction between the plasma and the keyhole, the laser beam is approximated as a parallel beam close to the surface of the welding plate. In the three-dimensional oscillation path.

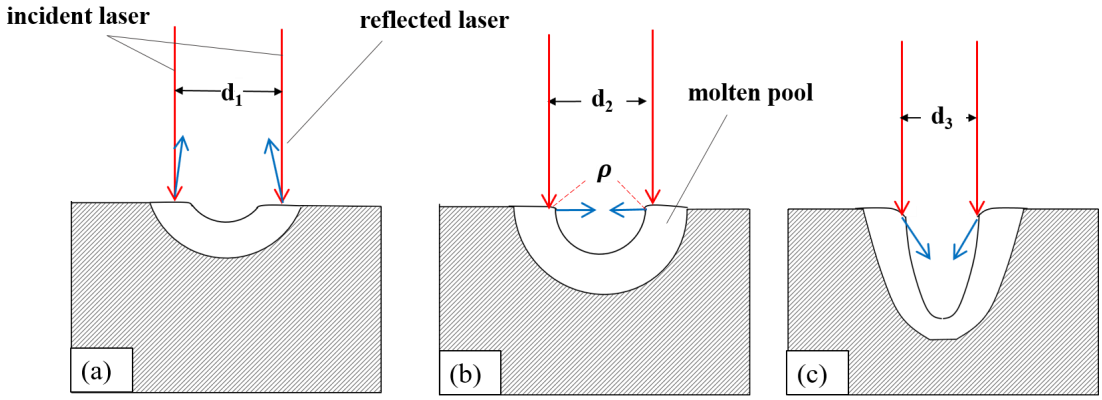


Fig 12. Schematic diagram of the welding mode change process.

As shown in Fig. 12, with the decrease of the spot diameter, the reflected laser beam changes from the upward direction to the horizontal direction, and then to the downward direction. In Fig. 12(b), the laser realizes self-focusing, which changes the absorption of laser energy in the molten pool from surface absorption to Fresnel absorption, greatly improves the efficiency of energy coupling, sharply increases the steam recoil pressure and

weld penetration, and the welding mode changes from heat-conduction mode to keyhole mode. Therefore, Fig. 12(b) shows the critical state of welding mode transition. Analyze the force balance of gas-liquid interface in molten pool under this state:

$$P_r \approx P_s \tag{9}$$

Where $P_r$ is vapor recoil pressure, $P_s$ is the surface tension. The gas-liquid interface in the critical state is approximated as an arc, and the following can be obtained:

$$P_s = \frac{2\sigma}{\rho_r} \tag{10}$$

$$\rho_r = \sqrt{2}\rho \tag{11}$$

In this paper, the $\rho$ is 0.5mm. .Since the Hertz-Langmuir relation (Samokhin, 1990) is only valid at high vaporization intensities (when temperature is much higher than boiling point or in vacuum), the $P_s$ is calculated by bridging the vaporization regimes with a smoothed third-order polynomial:

$$P_s = \begin{cases} P_0, & 0 \le T \le T_l \\ a_2T^3 + b_2T^2 + c_2T + d, & T_l \le T \le T_h \\ \frac{1}{2}\beta_R P_0 \exp\left(\frac{M_l L_v}{kT_v}\left(1 - \frac{T_v}{T}\right)\right) & T \ge T_h \end{cases} \tag{12}$$

Where $P_0$ represents atmospheric pressure, $M_l$ is the molar mass of the vaporized species, $L_v$ represents the latent heat of vaporization, the temperature thresholds $T_l$ and $T_h$ represent the low and high vaporization intensity regimes, and $T_v$ is the boiling point at atmospheric pressure, $k$ is the gas constant and numerically equal to the Boltzmann constant, $\beta_R$ is the retro-diffusion coefficient, $a_2, b_2, c_2, d$ are fitting coefficients. Although equation 12 is based on the Clausius-Clapeyron law, Lin et al. (2017) proposed that the recoil pressure is linearly related to the saturated vapor pressure. Using equation 8-11, the temperature at which the depression reaches a specific depth is obtained, through solving equations:

$$\begin{cases} a_2T^3 + b_2T^2 + c_2T + d = \frac{2\sigma}{\rho_r}, & T_l \le T \le T_h \\ \frac{1}{2}\beta_R P_0 \exp\left(\frac{M_l L_v}{kT_v}\left(1 - \frac{T_v}{T}\right)\right) = \frac{2\sigma}{\rho_r}, & T \ge T_h \end{cases} \tag{13}$$

In this study, the $T_l$ and $T_h$ are defined as evaporation temperature and boiling temperature respectively. Gan et al. (2021) ignored the coupling between temperature field governed equations and keyhole formation condition

in the linear welding. In this study, the normalization temperature of the melt pool at the center of the laser spot is calculated (equation 14 for the normalization method). The results of the one-way coupling of the temperature field control equation and the keyhole formation condition are graphically shown in Fig. 13(a1-a3), which ignore the positive effect of keyhole to laser energy absorption. The results of the two-way coupling of the temperature field control equation and the keyhole formation condition are graphically shown in Fig. 13(b1-b3). The coupling between temperature field and keyhole formation condition can be understood that the increase of temperature will lead to the formation of a keyhole, which in turn will further increase the temperature. Compared to the weld surface morphology in Fig. 13, it is clear that the two-way coupling calculation method (Fig. 13(b1-b3)) is more suitable in 3-d oscillation welding, and the former (Fig. 13(b1-b3)) takes the positive effect of the keyhole to laser energy absorption into consideration while the latter (Fig. 13(a1-a3)) does not.

$$T^* = \frac{T}{T_{th}} \times 100\% \tag{14}$$

$T_{th}$ represent the threshold of keyhole formation, obtained by solving equation 13. $T$ is the temperature of the melt pool at the center of the laser spot. $T^*$ is the normalization temperature.

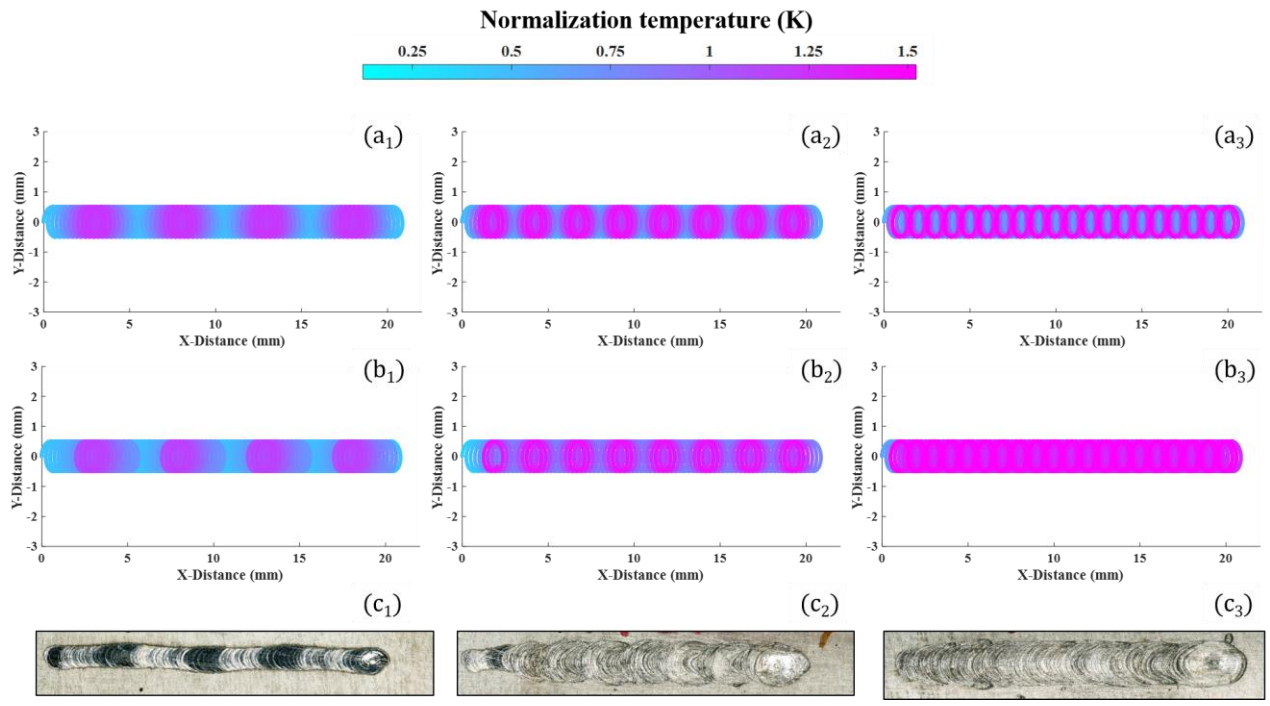


Fig 13. Compare the matching level of different calculation methods for surface morphologies; Results of previous method to calculate the normalized temperature ($a_1$-$a_3$); Results of present method to calculate the normalized temperature ($b_1$-$b_3$). Surface morphologies of $f_{xy} = 200\text{Hz}, f_z = 5\text{Hz}$ ($c_1$), $f_{xy} = 200\text{Hz}, f_z = 10\text{Hz}$ ($c_2$), $f_{xy} = 200\text{Hz}, f_z = 25\text{Hz}$ ($c_3$).

Two points are illustrated in this section. First, the reason for the shift in welding mode due to 3-d oscillation

is that the addition of vertical oscillation changes the energy distribution, causing the temperature at certain points higher than the temperature at the same point in 2-d oscillation. Second, a self-focus effect model is used to calculate the threshold for the keyhole welding mode, which matches the surface morphologies of the weld at low frequency oscillations better than previous methods.

3.3. Study of keyhole stability and porosity in 3-d oscillating welding

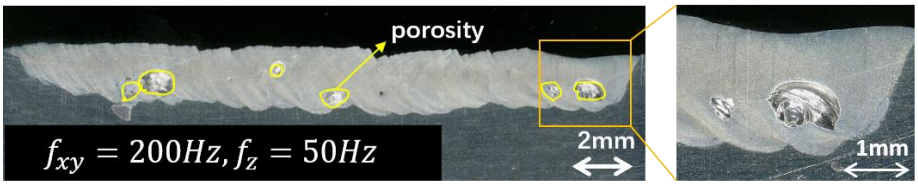


Fig 14. longitudinal sections of the weld ($f_{xy} = 200\text{Hz}, f_z = 50\text{Hz}$)

In Fig. 14, most of the pores are distributed in the middle and lower parts of weld. The pores have irregular shapes and obviously different sizes. Berger et al. (2011) announced that the above description of pore shape are characteristics of keyhole-induced pores. Hydrogen in the plate surface has been removed through chemical cleaning before welding and the weld pool is well protected, which prevents the formation of hydrogen pores from the source.

Two conclusions that descript the behavior of molten pool when the focus moves above the sample can be drawn by observing the video in the attachment 1: The first situation occurs in the low vertical oscillation frequency, the keyhole gradually disappears, and the welding mode returns to the heat-conduction welding mode, which can be seen as the reversed process of what is described in Fig. 12. In the second case, the keyhole tend to change but always exists because of the high vertical oscillation frequency. According to Ning et al. (2019), the disappearance of the deep keyhole takes some time because of the recoil pressure. Therefore, when the vertical oscillation frequency is on a high value, the keyhole would not disappear immediately.

Cheng et al. (2021) found that the spot often leads the keyhole in the extremely fast scanning speed. Fetzer et al. (2021) found that during high speed laser welding of aluminum alloys, energy absorption occurs mainly in the front wall. As is showed in Fig.14(b) and (c), in oscillation laser beam welding with high scanning speed over 2000 mm / s, the laser spot leads the keyhole. Lin et al. (2017) proved that laser energy deposition on the front wall of keyhole is beneficial to the stability of the keyhole by a CFD model. Since the three-dimensional oscillation is composed of the rotational oscillation in the XY-plane and the quasi-harmonic oscillation in the z direction, the actual linear velocity in the three-dimensional oscillation is also very high, and the relative position of the laser and

the keyhole is similar to that in the two-dimensional oscillation, as shown in the Fig. 15.

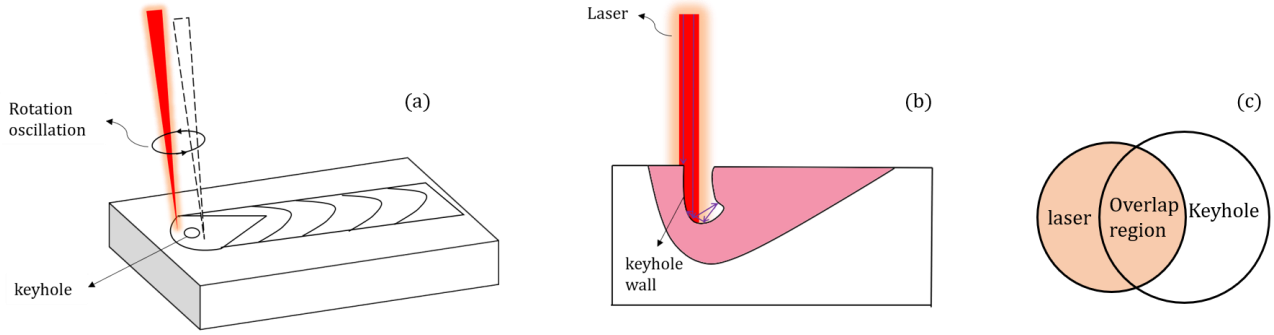


Fig 15. The schematic diagram of beam action in the case of small rotation oscillating amplitude. (a) basic view; (b) Section view; (c) overlap region between laser spot and keyhole inlet.

Furthermore, As is shown in Fig. 16 when the ratio of vertical oscillation frequency to the rotational is 1, the laser beam at the front keyhole wall is negatively defocused in the half cycle of oscillation. when the focus moves to point 0, it is in the maximum positive defocus position. When the focus moves from point 0 to point 1, the defocus amount decreases, and when it reaches point 1, the defocus becomes 0. When the focus moves from point 1 to point 2, the defocus amount continues to decrease, and when it reaches point 2, the defocus reaches the minimum value of - 2mm. This means that the keyhole absorbs positive defocused laser on the half cycle near the center of the molten pool and negative defocused laser on the other half.

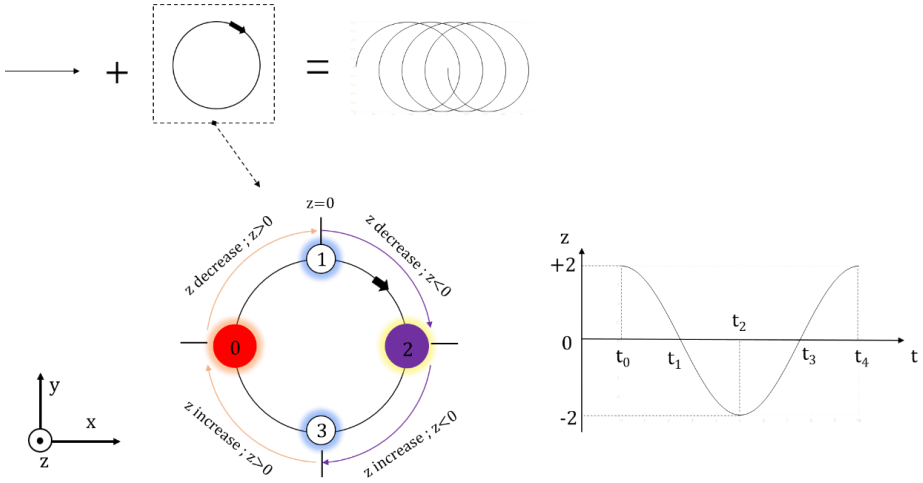


Fig 16. Schematic of the relationship between rotation oscillation and vertical oscillation

To study the stability of keyhole at different frequency ratios, Huang et al. (2018) used a “half sandwich

method" to observe the keyhole directly. In previous studies on keyhole behavior, Fetzer et al. (2018) indicated that keyholes with periodic fluctuations are the main cause of pores, and in our study, similar cases were collected in Fig. 17. A series of photos show that in some welds, the shape of capillary is changing and leaves pores in the weld. During 0ms~2ms, the bottom of the capillary expands. During 2ms~4ms, due to the surface tension effect, the expanded part separates from the capillary and becomes a bubble (Fetzer et al., 2018). This shows that the pore formation mechanism caused by unstable parameters in 3-d oscillation is similar to the traditional linear welding, which is formed by unstable keyhole collapse. In 3-d oscillation welding, lower level of keyhole depth fluctuation also means less porosity and more stable welding process. As shown in Figure 18, the keyhole depth is collected through high-speed photography. (Lin et al., 2017) claimed that the change of keyhole depth can moderately characterize the stability of keyhole. When the vertical oscillation frequency and rotation oscillation frequency are both 100 Hz, the change of keyhole depth is minimal, which means the keyhole is more stable at $f_z = 100\text{Hz}, f_{xy} = 100\text{Hz}$.

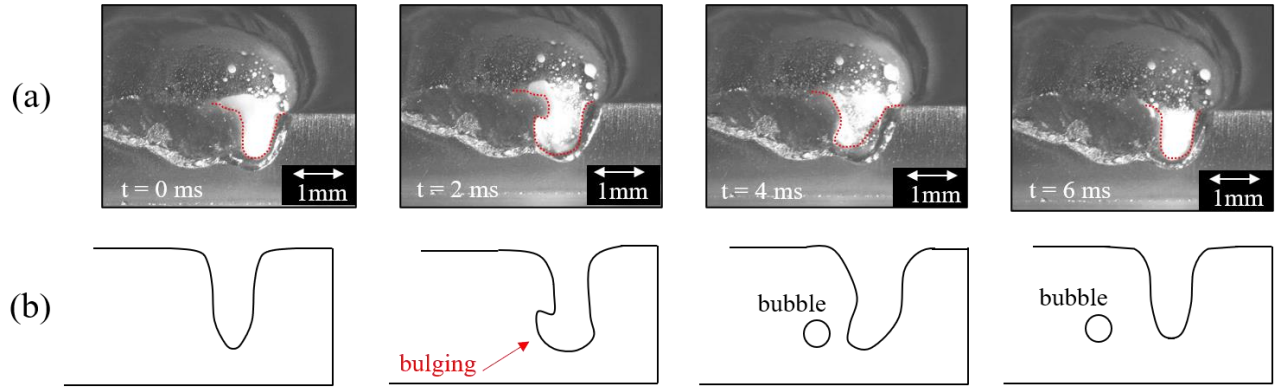


Fig 17. (a) CCD image of the keyhole ($f_z = 25Hz, f_{xy} = 200Hz$); (b)schematic diagram of the keyhole formation.

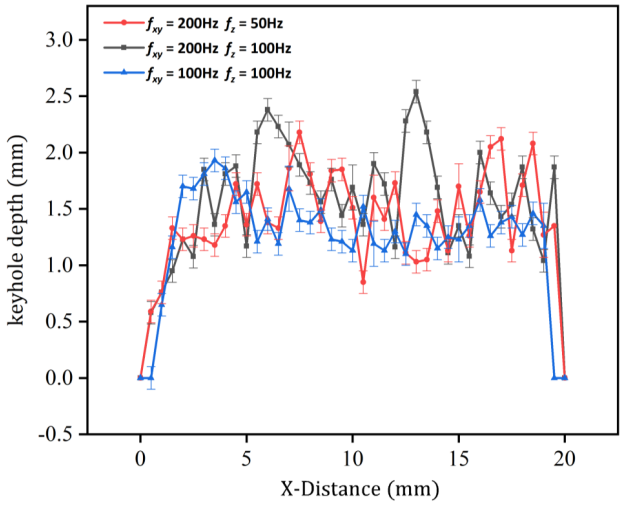


Fig 18. Curve of keyhole depth collected by high-speed photographic

Lin et al. (2017) proposed that the energy mainly concentrates on the front wall under high feed rate and high power of aluminum alloy, which is thought to reduce the flow velocity behind the molten pool. Fetzer et al. (2021) esteemed that the energy distribution in the keyhole had an important influence on the stability of the keyhole, and the experiment proved that the keyhole was more stable when the energy was mainly distributed in the front wall. Meanwhile, Zhao and DebRoy (2003) calculated the reflection of laser beam in keyhole and proposed that negative defocusing is thought to deepen keyhole depth by increasing laser absorption when defocusing is less than keyhole depth in aluminum alloy laser welding. In 3-d oscillation welding, when the ratio of vertical oscillation frequency to rotation oscillation frequency is 1, the laser on the front wall of the keyhole is negative defocusing, which causes high energy input and obtain a more stable welding process.

As is shown in Fig. 19, The porosity in the weld without oscillating is the largest, followed by that is the three-dimensional oscillating but vertical frequency is not equal to rotation frequency, and the porosity is the smallest when the two frequencies are equal. The result of X-ray radiographs is similar to the result of longitudinal section observation.

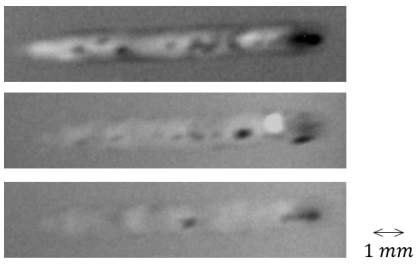


Fig. 19. X-ray radiographs (taken form the topside of the welds): (a) without beam oscillating (P = 3.68 kW); (b) 3-d laser beam oscillation ($f_z = 200Hz$, $f_{xy} = 100Hz$); (c) 3-d laser beam oscillation ($f_z = 100Hz$, $f_{xy} = 100Hz$)

According to the above discussions, to obtain welds with lower porosity in 3-d oscillation welding, the following points should be followed in process design: One is to avoid the keyhole in the unstable state as shown in Figure 4, which can be achieved by avoiding the welding parameters in the unstable state as calculated in 3.2. Another is to compare the porosity distribution of deep penetration welding under different oscillation frequency ratios. Welds based on the above two points are shown in Fig. 20. When the frequency is on $f_z$ = 50 Hz, $f_{xy}$ = 50 Hz, the porosity is 26% lower weld at the same vertical oscillation frequency and higher rotation oscillation. When the frequency is on $f_z$=100Hz, $f_{xy}$ = 100Hz, the porosity is 35% lower, and when the frequency is on $f_z$=200 Hz, $f_{xy}$ = 200 Hz, the porosity is 19% lower. The experimental results show that it is possible to change the energy distribution in keyhole by three-dimensional laser beam oscillation, which is meaningful to obtain aluminum alloy welds with low porosity at low power.

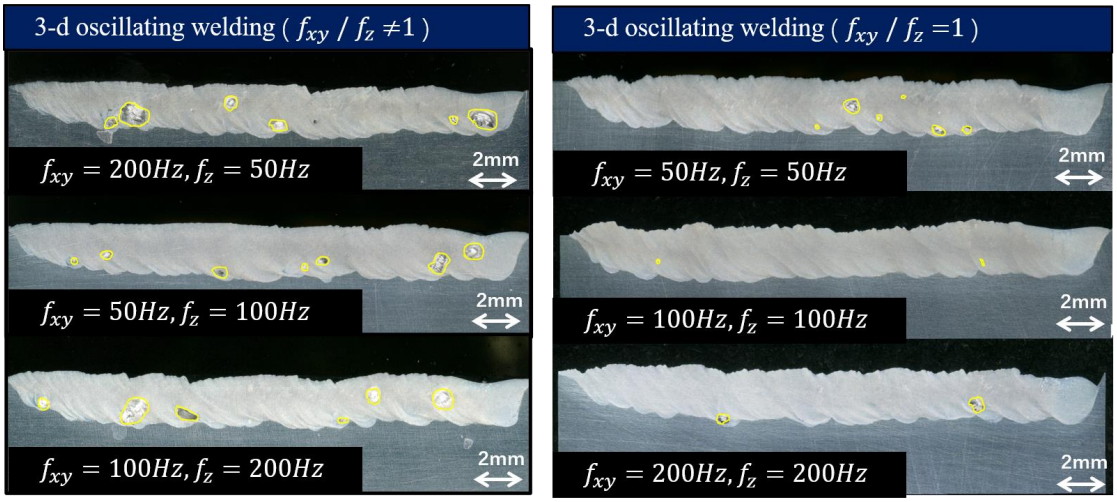


Fig 20. Transverse metallographic section with different frequency ratio.

## 4. Conclusion

In this paper, the welding mode transition window in 3-d laser beam oscillation welding has been investigated. The following conclusions can be drawn:

1. Previous 2-d (two-dimensional) oscillation welding has the disadvantage of dispersed heat input, which can only be welded in heat conduction mode at 3.68kW power and 3m/min feed rate. Adding vertical oscillation can effectively solve this problem. The experiment shows that laser beam 3-d (three-dimensional) oscillation can change the welding mode from heat-conduction mode to keyhole mode.

2. The accumulation of energy at some special points on the substrate causes the keyhole to appear at these points.

3. By analyzing the keyhole in the extreme state, a criterion model based on laser self-focus is used to calculate the threshold temperature in 3-d laser beam oscillation welding. The graphic of the normalized temperature shows that the model can accurately predict the transformation of heat-conduction mode and keyhole mode in 3-d oscillation welding.

4. The high-speed photographic observation of the weld implies that the laser was directly heating the walls of the keyhole. The experimental results show that it is possible to change the energy distribution in keyhole by three-dimensional laser beam oscillation, which is meaningful to obtain aluminum alloy welds with low porosity at low power and low feed rate. Next work plan: Quantitative calculation of keyhole energy distribution in laser beam 3-d oscillating welding by ray-tracing.

**Acknowledgments**

This research was supported by Natural Science Foundation of China (52075317), the Royal Society through International Exchanges 2018 Cost Share (China) scheme (IEC\NSFC\181278), Shanghai Science and Technology Committee Innovation Grant (19511106400, 19511106402), Shanghai Local Colleges and Universities Capacity Building Special Plan Project (19030501300).

## Reference

### Uncategorized References


Berger, P., Hügel, H., Graf, T., 2011. Understanding Pore Formation in Laser Beam Welding. Physics Procedia 12, 241-247.

Cheng, H., Zhou, L., Sun, J., Wen, S., Wang, Y., Chang, B., Du, D., 2021. Processing modes in laser beam oscillating welding of Al 6Cu alloy. Journal of Manufacturing Processes 68, 1261-1270.

Fetzer, F., Hagenlocher, C., Weber, R., Graf, T., 2021. Geometry and stability of the capillary during deep-penetration laser welding of AlMgSi at high feed rates. Optics & Laser Technology 133.

Fetzer, F., Sommer, M., Weber, R., Weberpals, J.-P., Graf, T., 2018. Reduction of pores by means of laser beam oscillation during remote welding of AlMgSi. Optics and Lasers in Engineering 108, 68-77.

Gan, Z., Kafka, O.L., Parab, N., Zhao, C., Fang, L., Heinonen, O., Sun, T., Liu, W.K., 2021. Universal scaling laws of keyhole stability and porosity in 3D printing of metals. Nat Commun 12, 2379.

Graf, T., Berger, P., Weber, R., Hügel, H., Heider, A., Stritt, P., 2015. Analytical expressions for the threshold of deep-penetration laser welding. Laser Physics Letters 12.

Hao, K., Li, G., Gao, M., Zeng, X., 2015. Weld formation mechanism of fiber laser oscillating welding of austenitic stainless steel. Journal of Materials Processing Technology 225, 77-83.

Huang, L., Hua, X., Wu, D., Fang, L., Cai, Y., Ye, Y., 2018. Effect of magnesium content on keyhole-induced porosity formation and distribution in aluminum alloys laser welding. Journal of Manufacturing Processes 33, 43-53.

Jia, Z., Zhang, P., Yu, Z., Wu, D., Tian, Y., Yan, H., 2021. Evidence of solidification crack propagation in pulsed laser welding of aluminum alloy. Opt Express 29, 18495-18501.

Jiang, Z., Chen, X., Li, H., Lei, Z., Chen, Y., Wu, S., Wang, Y., 2020. Grain refinement and laser energy distribution during laser oscillating welding of Invar alloy. Materials & Design 186.

Ke, W., Bu, X., Oliveira, J.P., Xu, W., Wang, Z., Zeng, Z., 2021. Modeling and numerical study of keyhole-induced porosity formation in laser beam oscillating welding of 5A06 aluminum alloy. Optics & Laser Technology 133.

Kumar, N., Das, A., Dale, T., Masters, I., 2021. Laser wobble welding of fluid-based cooling channel joining for battery thermal management. Journal of Manufacturing Processes 67, 151-169.

Lin, R., Wang, H.-p., Lu, F., Solomon, J., Carlson, B.E., 2017. Numerical study of keyhole dynamics and keyhole-induced porosity formation in remote laser welding of Al alloys. International Journal of Heat and Mass Transfer 108, 244-256.

Martin, A.A., Calta, N.P., Khairallah, S.A., Wang, J., Depond, P.J., Fong, A.Y., Thampy, V., Guss, G.M., Kiss, A.M., Stone, K.H., Tassone, C.J., Nelson Weker, J., Toney, M.F., van Buuren, T., Matthews, M.J., 2019. Dynamics of pore formation during laser powder bed fusion additive manufacturing. Nat Commun 10, 1987.

Ning, J., Zhang, L.-J., Yin, X.-q., Zhang, J.-X., Na, S.-J., 2019. Mechanism study on the effects of power modulation on energy coupling efficiency in infrared laser welding of highly-reflective materials. Materials & Design 178.

Rodrigues, N., Oliveira, E., Leitão, P., 2018. Decentralized and on-the-fly agent-based service reconfiguration in manufacturing systems. Computers in Industry 101, 81-90.

Samokhin, A.J.P.o.t.I.o.G.P.A.o.S.o.t.U.S.E.A.P., 1990. Effect of laser radiation on absorbing condensed matter. 13, 203.

Stritt, P., Weber, R., Graf, T., Müller, S., Ebert, C., 2011. Utilizing Laser Power Modulation to Investigate the Transition from Heat-Conduction to Deep-Penetration Welding. Physics Procedia 12, 224-231.

Tsay, L.W., Shan, Y.P., Chao, Y.H., Shu, W.Y., 2006. The influence of porosity on the fatigue crack growth behavior

of Ti–6Al–4V laser welds. Journal of Materials Science 41, 7498-7505.

Wang, Z., Oliveira, J.P., Zeng, Z., Bu, X., Peng, B., Shao, X., 2019. Laser beam oscillating welding of 5A06 aluminum alloys: Microstructure, porosity and mechanical properties. Optics & Laser Technology 111, 58-65.

Wu, Q., Xiao, R.S., Zou, J.L., Xu, J.J., 2018. Weld formation mechanism during fiber laser welding of aluminum alloys with focus rotation and vertical oscillation. Journal of Manufacturing Processes 36, 149-154.

Zhang, C., Li, X., Gao, M., 2020a. Effects of circular oscillating beam on heat transfer and melt flow of laser melting pool. Journal of Materials Research and Technology 9, 9271-9282.

Zhang, C., Yu, Y., Chen, C., Zeng, X., Gao, M., 2020b. Suppressing porosity of a laser keyhole welded Al-6Mg alloy via beam oscillation. Journal of Materials Processing Technology 278.

Zhao, H., DebRoy, T., 2003. Macroporosity free aluminum alloy weldments through numerical simulation of keyhole mode laser welding. Journal of Applied Physics 93, 10089-10096.

Zou, J.L., He, Y., Wu, S.K., Huang, T., Xiao, R.S., 2015. Experimental and theoretical characterization of deep penetration welding threshold induced by 1-μm laser. Applied Surface Science 357, 1522-1527.

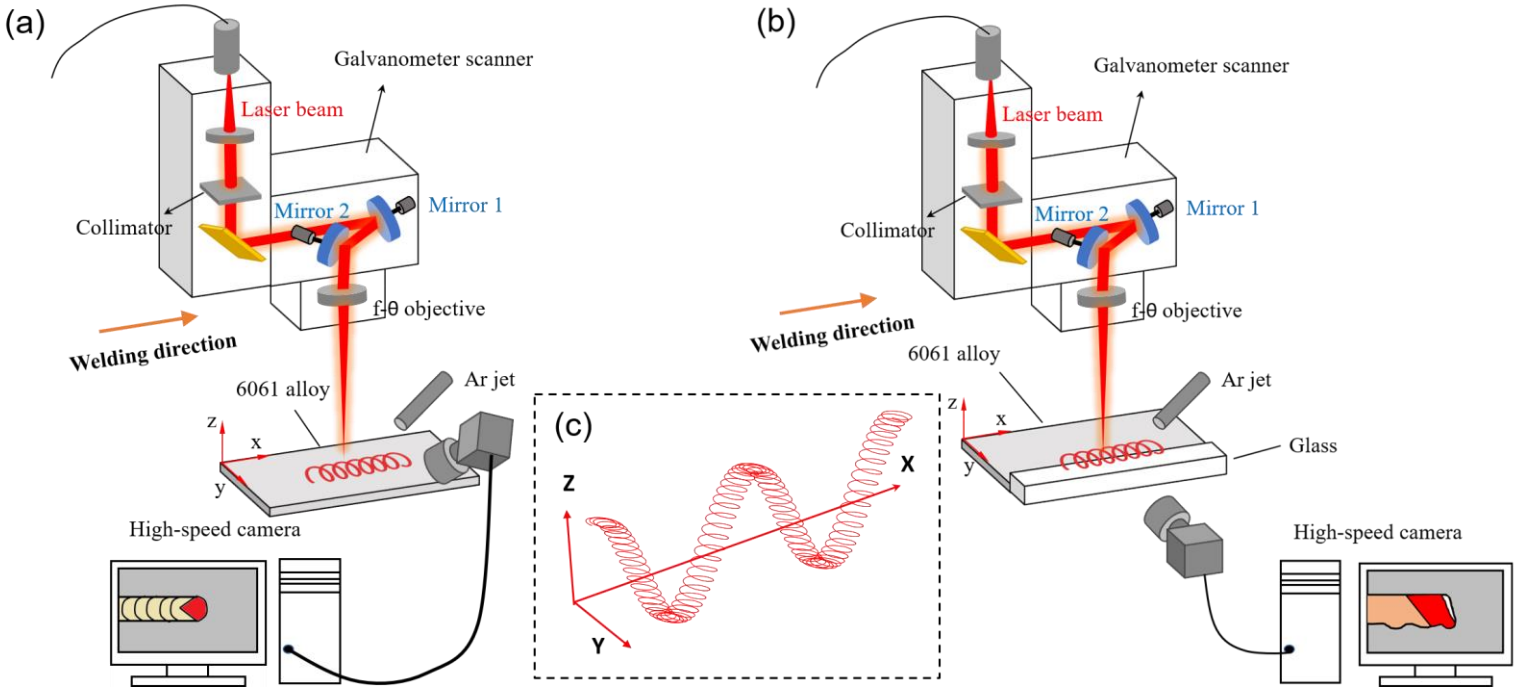


Fig 1. Schematic of the experimental setup and 3-d laser beam oscillating trajectory. (a) weld pool observation; (b) keyhole observation based on the " half sandwich" model; (c) 3-d laser oscillating trajectory.

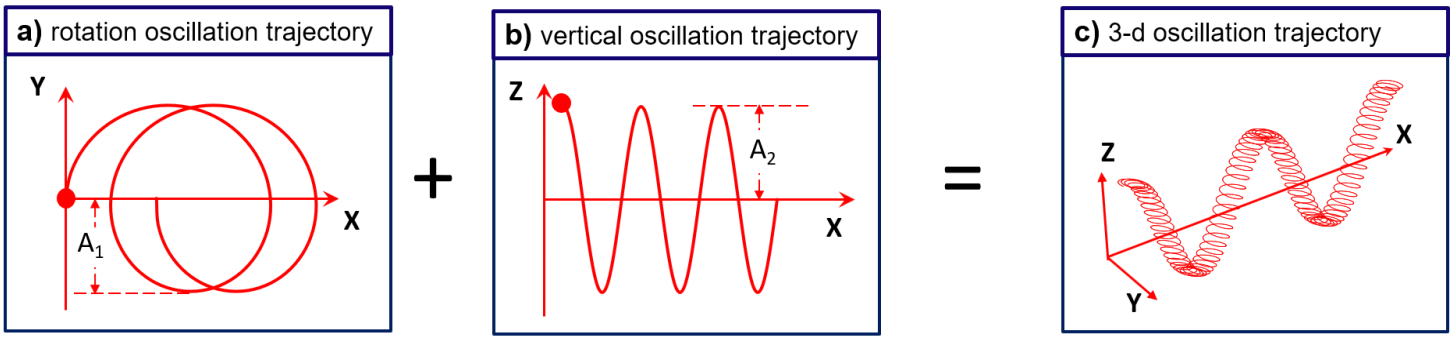


Fig 2. Process of inferring the 3-d oscillation trajectory.

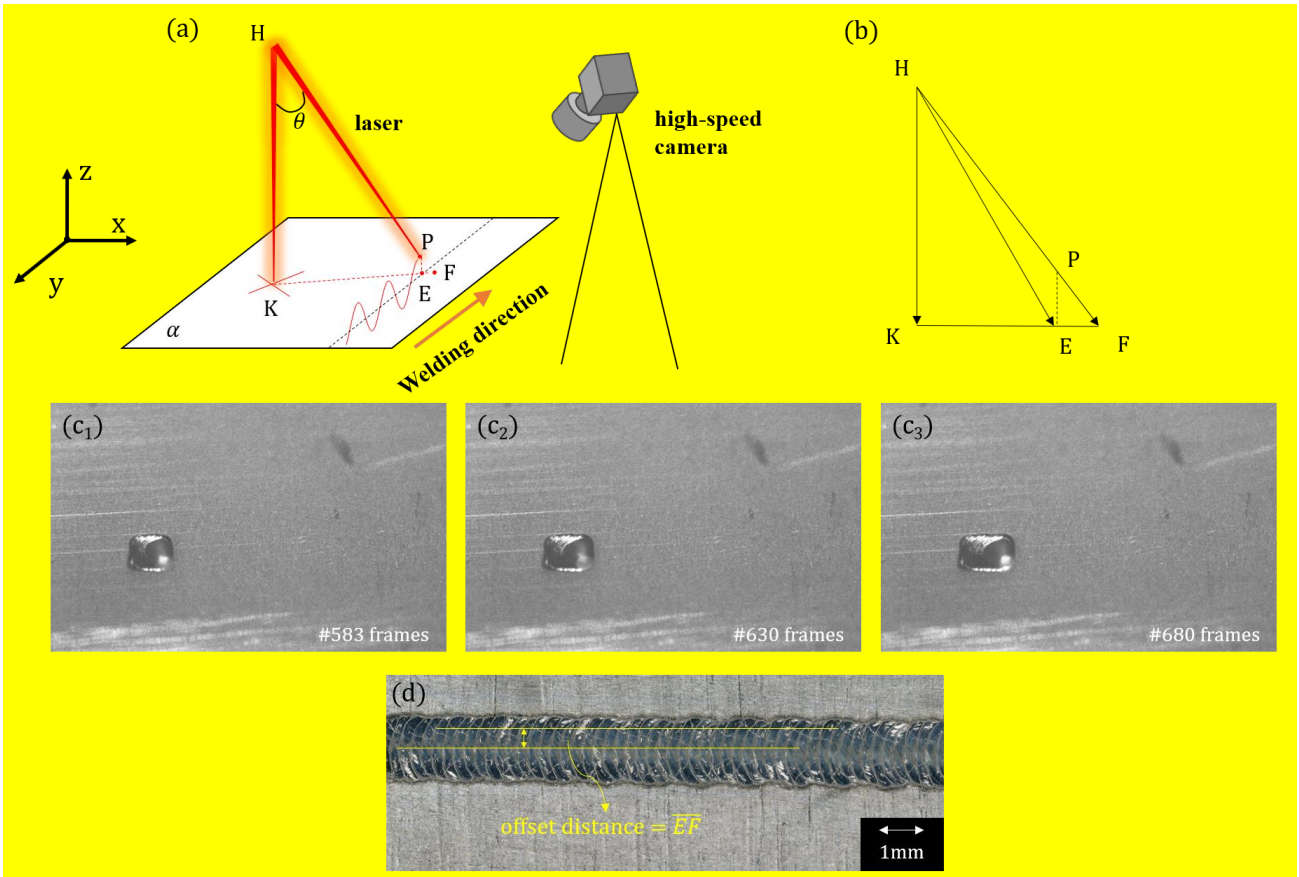


Fig 3. Schematic diagram and result of a confirmatory experiment about amplitude and frequency in vertical oscillation. (a) Schematic diagram; (b) geometric relationship between offset distance and oscillation amplitude; ($c_1$-$c_3$) Snapshot of high-speed video during two oscillation cycles; (d) weld surface morphology used to calculated the actual amplitude.

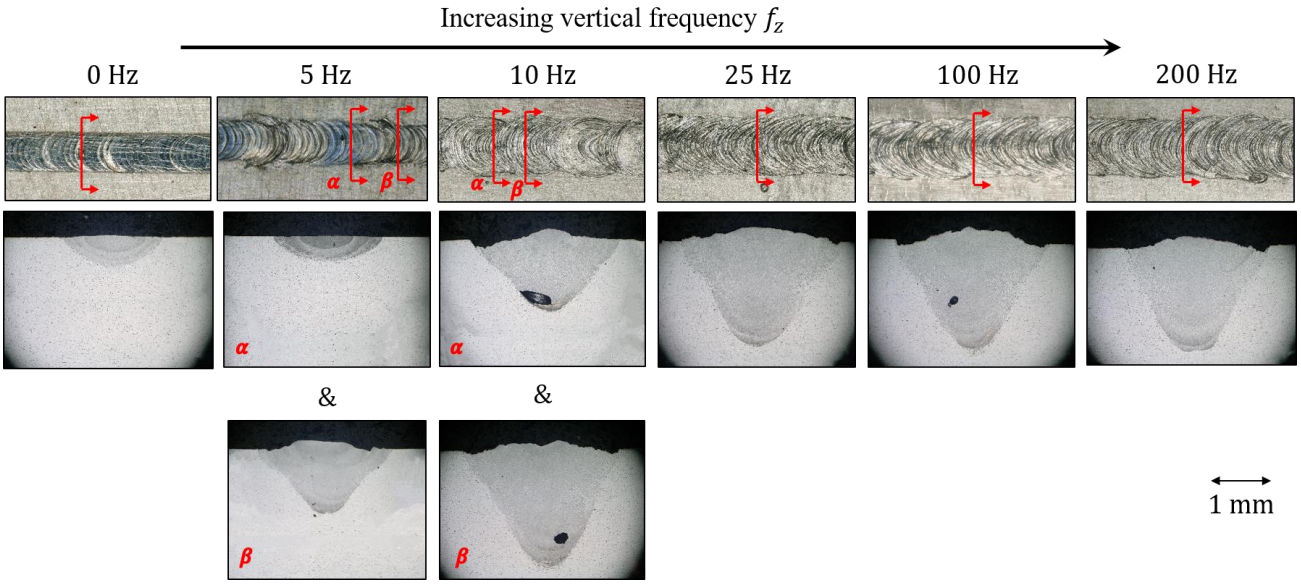


Fig 4. Morphologies of top surface and cross-section at the different vertical oscillating frequencies

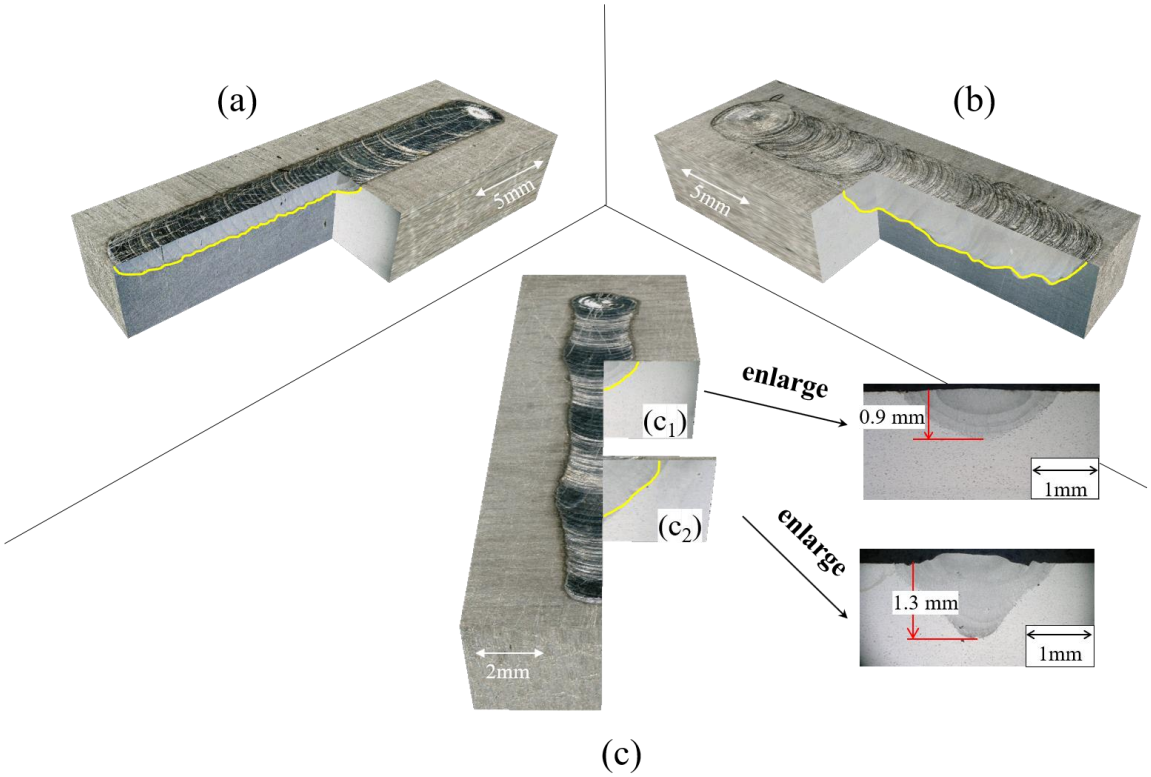


Fig 5. Three mode in the weld of laser beam 3-d oscillating, and metallographic section; (a) heat-conduction mode ($f_z = 0Hz$, $f_{xy} = 200$Hz); (b) keyhole mode ($f_z = 200$Hz, $f_{xy} = 200$Hz); (c) switching between heat-conduction mode and keyhole mode (SBHK mode) ($f_z = 5$Hz, $f_{xy} = 200$Hz)

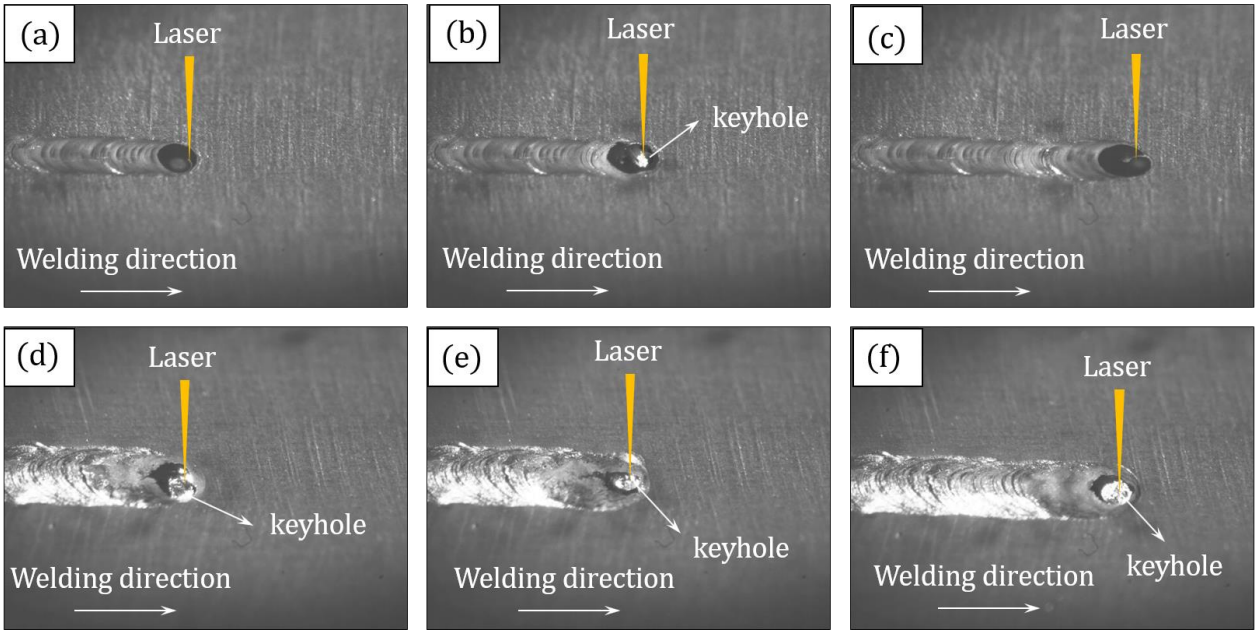


Fig 6. High speed photographs of the weld pool. vertical oscillating frequency $f_z = 5$Hz, rotation oscillating frequency $f_{xy} = 200$Hz in (a)-(c). vertical oscillating frequency $f_z = 25$Hz, rotation oscillating frequency $f_{xy} = 200$Hz in (d)-(f). (a) $t$ = 0.1875 s; (b) $t$ = 0.2125 s; (c) $t$ = 0.245 s; (d) $t$ = 0.1875 s; (e) $t$ = 0.2125 s; (f) $t$ = 0.245 s.

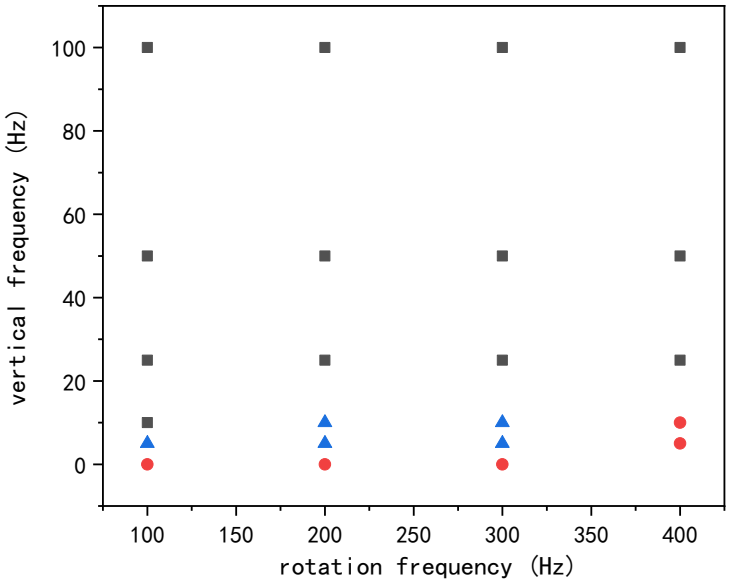


Fig. 7 Relationship between the oscillating frequency and welding mode. The square points represent the welding is on keyhole mode; The circular points represent the welding is on heat-conduction mode; The triangle points represent the welding is switching between heat-conduction mode and keyhole mode.

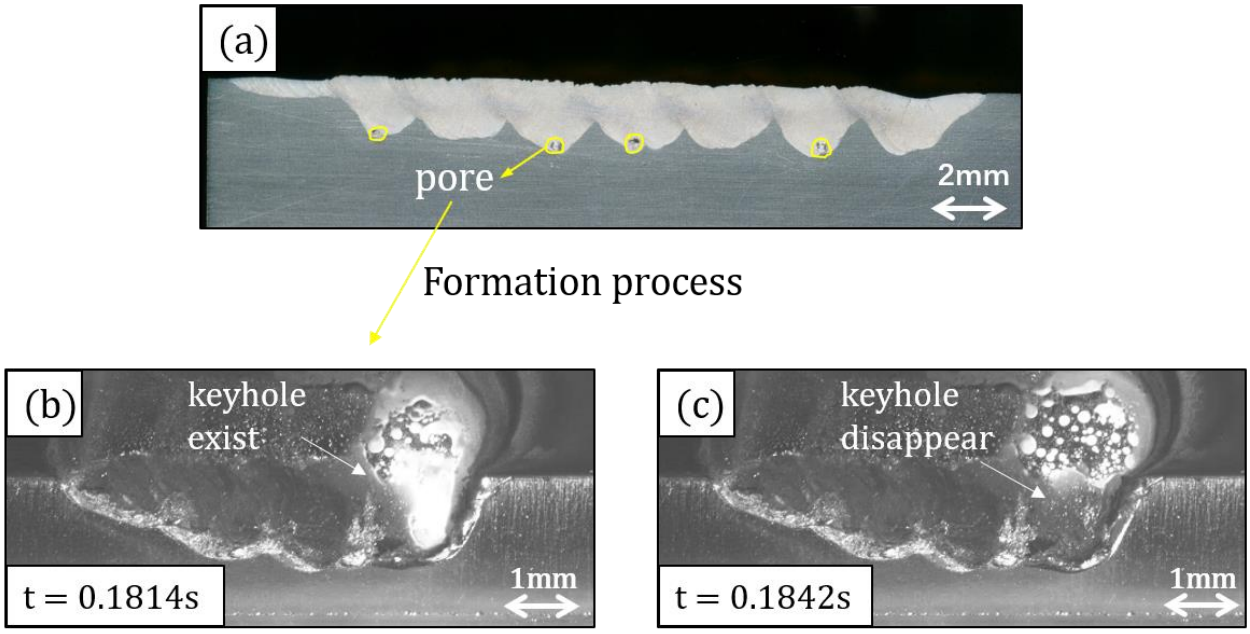


Fig. 8 Formation process of porosity when the welding is on SBHK mode (switching between heat-conduction mode and keyhole mode), the vertical oscillation frequency $f_z$ is 10Hz, the rotation oscillation frequency $f_{xy}$ is 200Hz

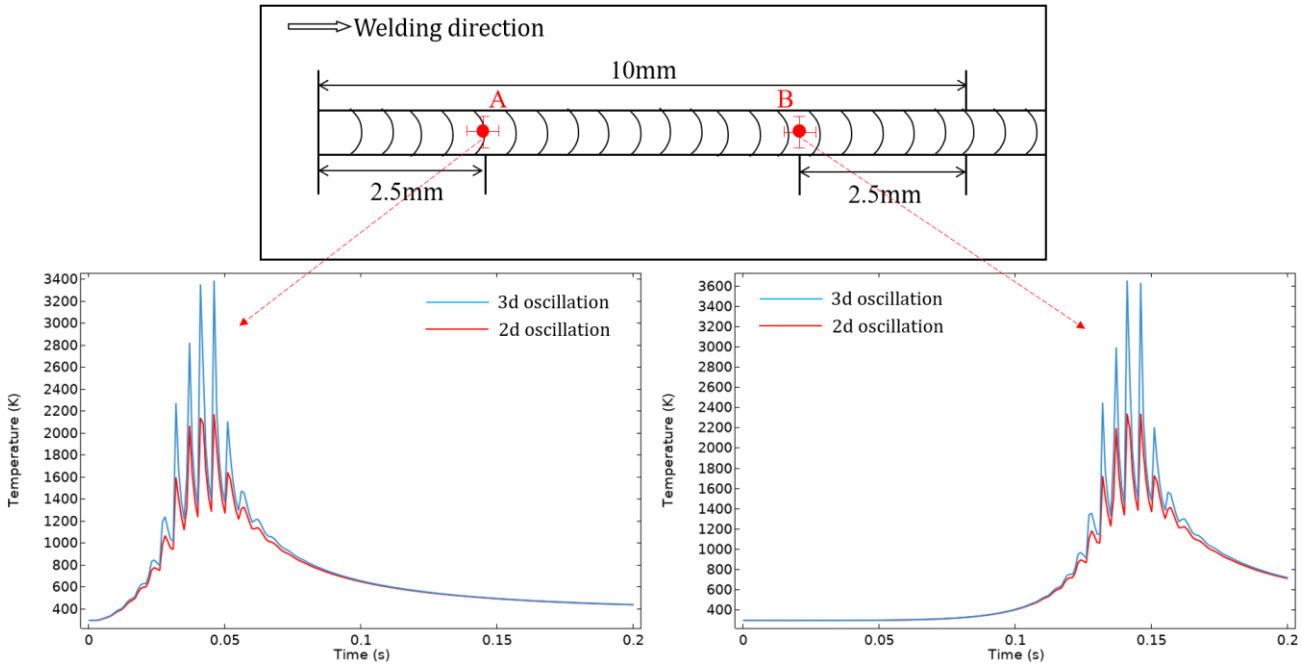


Fig 9. Temperature curve of point A and point B with different kind of laser oscillation.

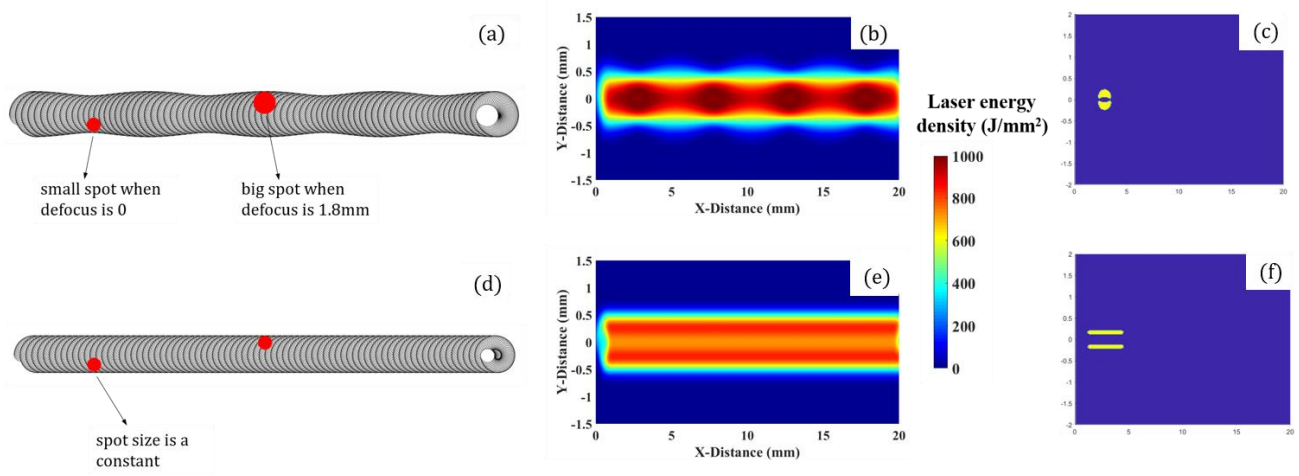


Fig 10. (a) Schematic diagram of the change of spot size in 3-d oscillation welding ($f_{xy}$= 200 Hz, $f_z$= 5 Hz); (b) Energy distribution in the weld of 3-d oscillation ($f_{xy}$= 200 Hz, $f_z$ = 5 Hz); (c) The area in 3-d oscillation laser beam welding, in which the energy density is larger than 700 J/mm2 (d) Schematic diagram of the change of spot size in 2-d oscillation welding ($f_{xy}$ = 200 Hz, $f_z$ = 0 Hz); (e) Energy distribution in the weld of 2-d oscillation ($f_{xy}$ = 200 Hz, $f_z$ = 0 Hz); (f) The area in 2-d oscillation laser beam welding, in which the accumulated energy is larger than 700 J/mm$^2$

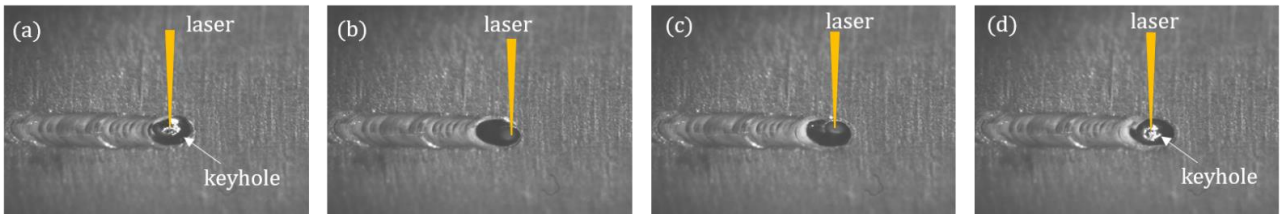


Fig 11. High-speed photography of molten pool during keyhole formation (a) 0.22 s; (b) 0.225 s; (c) 0.23s; (d) 0.235s.

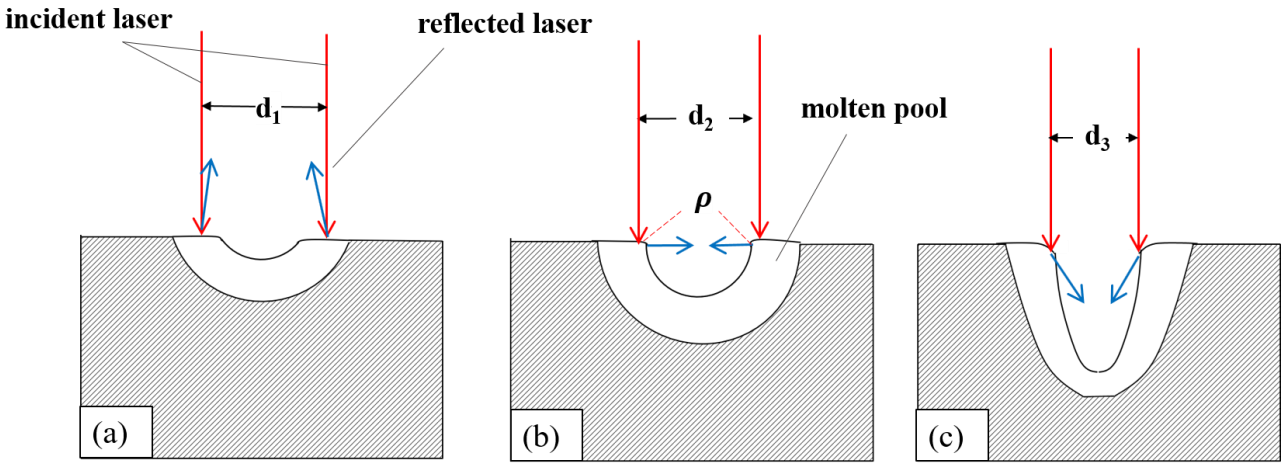


Fig 12. Schematic diagram of the welding mode change process.

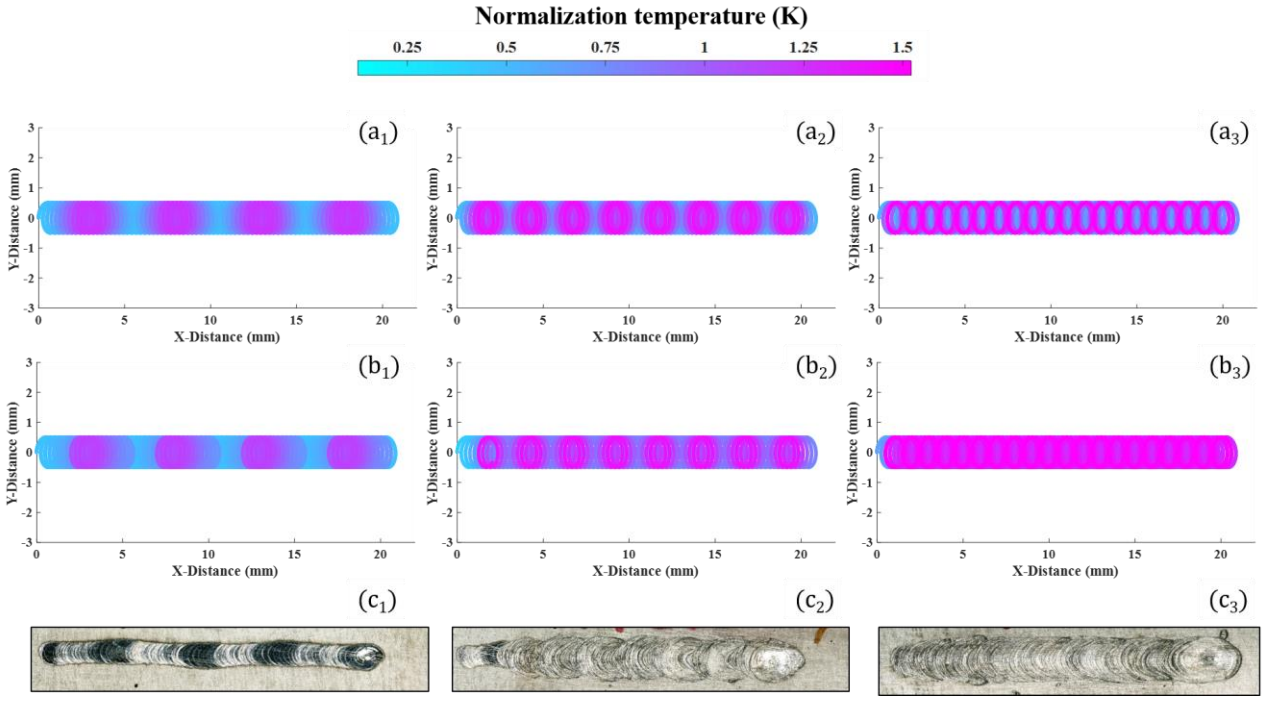


Fig 13. Compare the matching level of different calculation methods for surface morphologies; Results of previous method to calculate the normalized temperature ($a_1$-$a_3$); Results of present method to calculate the normalized temperature ($b_1$-$b_3$). Surface morphologies of $f_{xy} = 200\text{Hz}, f_z = 5\text{Hz}$ ($c_1$), $f_{xy} = 200\text{Hz}, f_z = 10\text{Hz}$ ($c_2$), $f_{xy} = 200\text{Hz}, f_z = 25\text{Hz}$ ($c_3$)

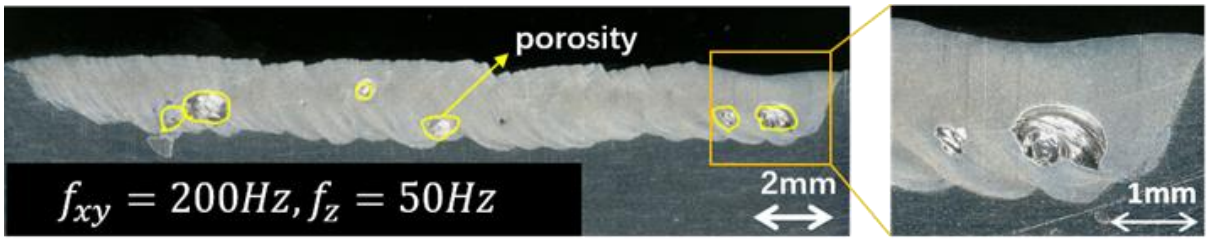


Fig 14. longitudinal sections of the weld $(f_{xy} = 200\text{Hz}, f_z = 50\text{Hz})$

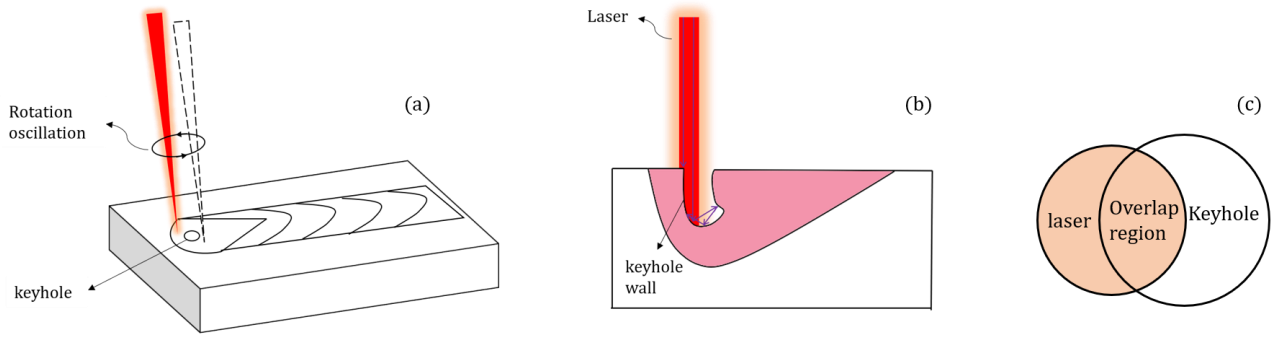


Fig 15. The schematic diagram of beam action in the case of small rotation oscillating amplitude. (a) basic view; (b) Section view; (c) overlap region between laser spot and keyhole inlet.

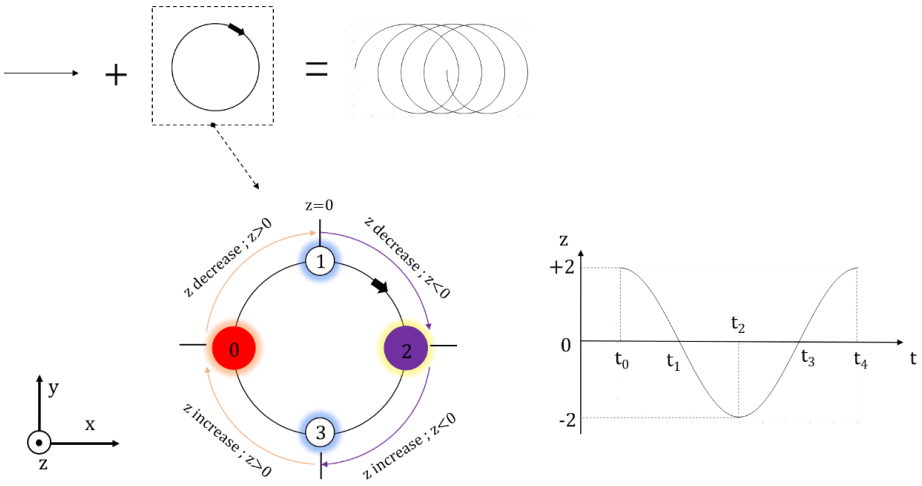


Fig 16. The schematic diagram of beam action in the case of small rotation oscillating amplitude. (a) basic view; (b) Section view.

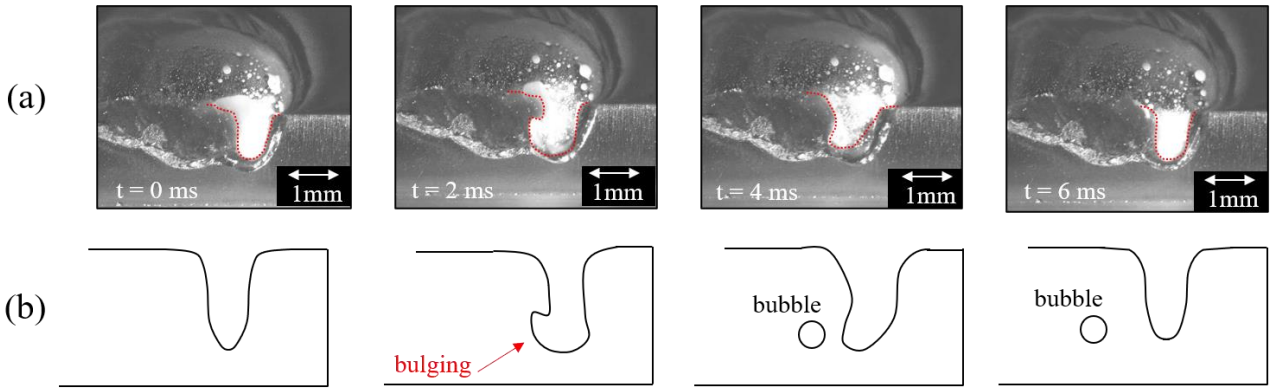


Fig 17. (a) CCD image of the keyhole ($f_z = 25Hz$, $f_{xy} = 200Hz$); (b)schematic diagram of the keyhole formation.

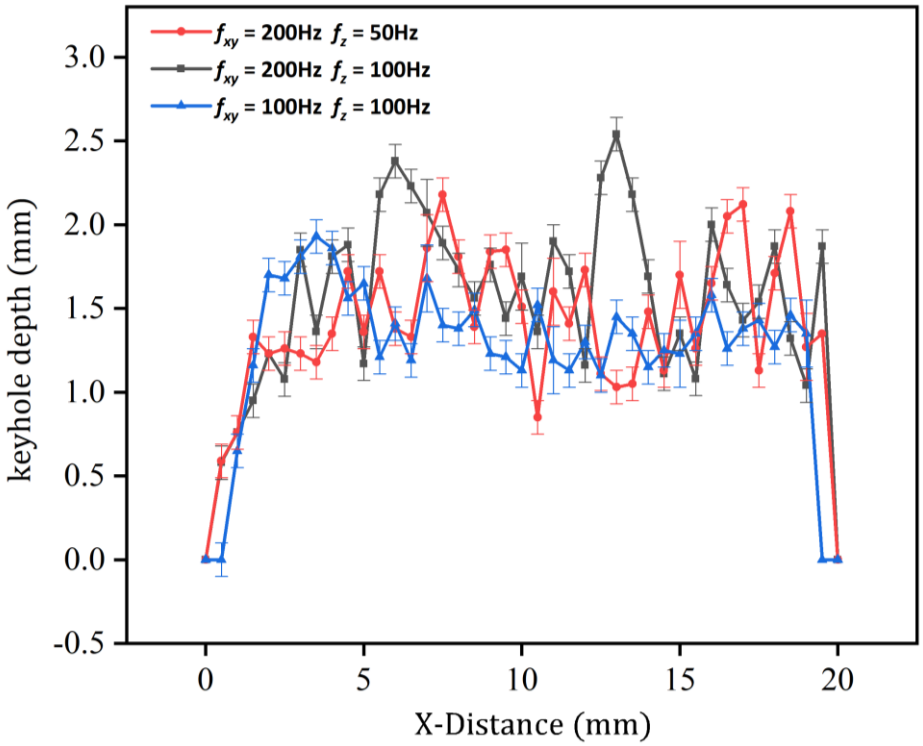


Fig 18. Curve of keyhole depth collected by high-speed photographic

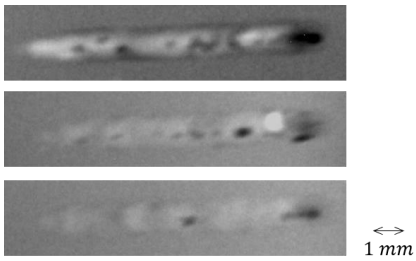


Fig. 19. X-ray radiographs (taken form the topside of the welds): (a) without beam oscillating (P = 3.68 kW); (b) 3-d laser beam oscillation ($f_z = 200Hz$, $f_{xy} = 100Hz$); (c) 3-d laser beam oscillation ($f_z = 100Hz$, $f_{xy} = 100Hz$)

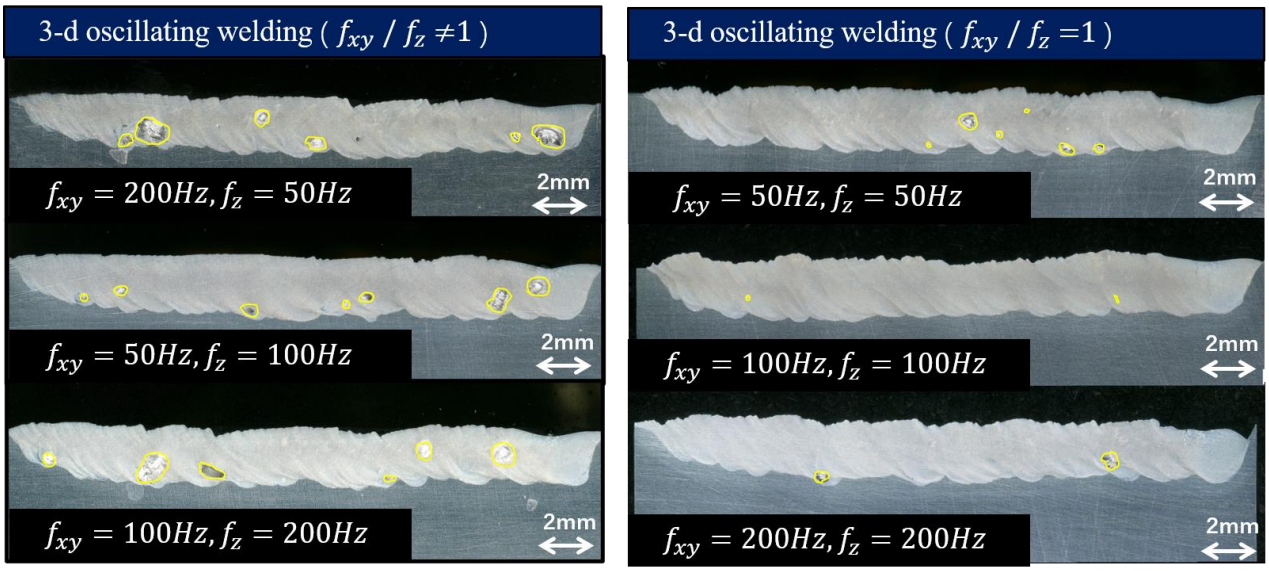


Fig 20. Transverse metallographic section with different frequency ratio.